SLAC-PUB-1038
(TH) and (EXP)
May 1972

Q^0 and $\bar{Q}^0$ PRODUCTION IN $K_L^0 p$ INTERACTIONS FROM 4 to 12 GeV/c *

G. W. Brandenburg, A. D. Brody,** W. B. Johnson, D.W.G.S. Leith, J. S. Loos, G. J. Luste,*** J.A.J. Matthews, K. Moriyasu,† B. C. Shen,†† W. M. Smart,††† F. C. Winkelmann, and R. J. Yamartino

Stanford Linear Accelerator Center
Stanford University, Stanford, California 94305

ABSTRACT

Experimental results are presented on the reactions $K^0 p \to Q^0 p$ and $\bar{K}^0 p \to \bar{Q}^0 p$ observed in the final state $K_S^0 \pi^+ \pi^- p$ in the momentum range 4 to 12 GeV/c. The data were acquired by exposing the SLAC 40-inch (1 meter) hydrogen bubble chamber to a neutral beam. Special emphasis is placed on a detailed comparison of the production characteristics of the two strangeness states. Cross sections, differential cross sections, density matrix elements, $K^*\pi$ mass spectra, and exponential slopes of the momentum transfer distributions are presented for $Q^0 p$ and $\bar{Q}^0 p$. An important result of this study is the observation of a crossover at $-t' = 0.13 \pm 0.03$ GeV^2 in the differential cross sections. We find that this effect is explained in analogy to elastic scattering by assuming that Regge, as well as Pomeron, exchange contributes to Q production. Calculations with a Reggeized Deck model are also made and we find that such models, as presently formulated, cannot explain the observed behavior of the differential cross sections or the energy dependence of the Q cross section.

*Work supported by the U. S. Atomic Energy Commission.
**Now at Sheffield University, Sheffield, Yorkshire, England.
***Now at the University of Toronto, Toronto, Canada.
†Now at the University of Washington, Seattle, Washington.
††Now at the University of California (Riverside), Riverside, California.
†††Now at the National Accelerator Laboratory, Batavia, Illinois.

(Submitted to Nucl. Phys. B.)

1. Introduction

The Q meson, which appears as a broad enchancement in the $K\pi\pi$ mass spectrum centered near 1.30 GeV, has been the subject of much experimental investigation both for Q^+ and Q^- production.[1,2] Although many properties of the Q enhancement have been established by these studies, it is still not known whether the Q is resonant or nonresonant or even whether it is a single object.[3,4] Likewise, the production mechanisms for the Q are not well understood, although reasonably successful descriptions of the data have been obtained in terms of diffraction dissociation[5] or the Deck effect.[6]

In this paper we suggest that a better understanding of the Q enhancement can be obtained by accurate comparisons of the reactions $Kp \to Qp$ and $\bar{K}p \to \bar{Q}p$. The difference between the differential cross sections for Qp and $\bar{Q}p$ (ref. 7) provides particularly interesting information on the production amplitudes in analogy to recent analyses of particle and antiparticle elastic scattering ($Xp \to Xp$ and $\bar{X}p \to \bar{X}p$).[8,9] Unfortunately, comparisons of published data on Q^+p and Q^-p are hampered by the uncertainties introduced by differences in absolute normalization and in analysis techniques.

In the present $K^o_L p$ experiment the equal components of K^o and $\bar{K}^o$ in the beam allow a precise comparison of the reactions

$$K^o p \to Q^o p$$

and

$$\bar{K}^o p \to \bar{Q}^o p \ ,$$

free from relative normalization problems. These reactions are observed over the interval 4 to 12 GeV/c in the final state

$$K^o_L p \to K^o_S \pi^+ \pi^- p \quad . \tag{1}$$

Details of the experiment are discussed in sect. 2.

In sect. 3 we report the results of our experiment. After presenting some of the general features of reaction (1), we define the "Q region" for our analysis, discuss the separation of Q^o and $\bar{Q}^o$, and give an account of procedures used to deal with background events in the Q signal. Then comparisons are made between the Q^o and $\bar{Q}^o$ mass spectra, production cross sections, differential cross sections, and density matrix elements. The results are briefly compared to those of other diffraction dissociation processes and to elastic scattering.

The implications of the data are discussed in sect. 4. Particular emphasis is placed on the analogy to elastic scattering in order to obtain an estimate of the Regge contribution to Q production. The predictions of a Reggeized Deck model[10,11] are then examined in light of the observed differences between Q^o and $\bar{Q}^o$ production.

A summary of our conclusions is given in sect. 5.

2. Experimental Details

2.1 Bubble Chamber Exposure and the K_L^o Beam

The data were obtained by exposing the SLAC 40-inch (1 meter) hydrogen-filled bubble chamber to a neutral beam of K_L^o mesons. The analysis for reaction (1) has been carried out on 800,000 photographs representing 32 events/μb. The number of observed events as a function of K_L^o beam momentum is given in table 1 and totals close to 10,000.

The K_L^o beam[12,13] was produced by impinging the primary electron beam (typically in the energy range from 16 to 19 GeV) onto a beryllium target located 55 meters upstream of the bubble chamber. Charged particles were magnetically swept out of the beam and photons were removed by placing a suitable amount of material immediately downstream of the target. The halo of muons was absorbed by ~ 15 meters of iron shielding placed around the

neutral beam channel. The K_L^o beam was collimated to have a cross-sectional area of 15 cm by 40 cm at the bubble chamber. For individual events the direction of the incident K_L^o particle is accurately determined by the position of the interaction within the chamber relative to the target position.

Both the shape and the absolute magnitude of the K_L^o momentum spectrum at the bubble chamber have been determined from the visible decays $K_L^o \to \pi^{\pm} e^{\mp} \nu$, $K_L^o \to \pi^{\pm} \mu^{\mp} \nu$, and $K_L^o \to \pi^+ \pi^- \pi^o$. The shape of the momentum spectrum, shown in fig. 1, has been deduced through an iterative procedure[12,13] using the experimental distribution of the variable P_{VIS}, defined as:

$$P_{VIS} = (\underset{\sim}{P}_1 + \underset{\sim}{P}_2) \cdot \underset{\sim}{n},$$

where $\underset{\sim}{P}_1$ and $\underset{\sim}{P}_2$ are the momenta of the two charged decay products and $\underset{\sim}{n}$ is the unit vector along the incident beam direction. The flags shown on the spectrum indicate the statistical spread of solutions obtained by our procedure and vary from 2% at 4 GeV/c to 15% at 12 GeV/c. The absolute magnitude of the beam flux is fixed by the K_L^o lifetime and the branching ratio $(K_L^o \to \text{neutrals})/(K_L^o \to \text{all})$.

2.2 Scanning and Measuring Procedures

The entire film sample was scanned for vee events. Events for reaction (1) belong to the "3-prong-vee" category whereas decays of the K_L^o beam belong to the "unassociated vee" category. A second scan was done for 10% of the film in order to establish scanning efficiencies (90 ± 5% for both categories). Measurements were done both on film plane digitizers and on the SLAC spiral reader with no apparent differences in accuracy. Especially difficult events were remeasured on the film plane machines. The programs TVGP and SQUAW were used for spatial reconstruction and kinematic fitting.

Care was taken to insure the correct association of vees to interactions. In cases of doubtful association of a vee, the scanners were instructed to assign the vee to "n-prong-vee" categories rather than to the "unassociated vee" category. After measurement of all "n-prong-vee" events, those vees which were really K_L^o beam decays were identified and reassigned (this amounted to a 10% increase in the number of K_L^o beam decays). Similarly, a fraction of the events measured as "unassociated vees" appeared to be K_S^o or Λ^o decays. These vees were then reexamined at the scan table to search for an associated interaction. This procedure increased the sample of events for reaction (1) by 2%.

2.3 Selection of the Events for $K_L^o p \rightarrow K_S^o \pi^+ \pi^- p$

These events have six kinematic constraints (three each for the interaction vertex and the decay vertex) and consequently form a well separated sample of data with less than 2% of the events being kinematically ambiguous with other K_S^o or Λ^o hypotheses. For the ambiguous events, the $K_S^o \pi^+ \pi^- p$ hypothesis has been chosen whenever it has the higher χ^2 probability. In addition, the χ^2 probability is required to exceed 1% for all events selected for further study.

A reduced interaction volume was imposed on the events in order to assure uniform detection efficiencies for the K_S^o decays. An event was excluded if the interaction occurred within 30 cm, or if the decay occurred within 15 cm, of the downstream end of the chamber. These restrictions provided a minimum of 15 cm for the K_S^o decay path as well as a minimum of 15 cm (30 cm) for measurement of the tracks from the decay (interaction) vertex. Events were also discarded whenever the distance between interaction and K_S^o decay was less than 0.75 cm. The accepted events then were given a weight, W, equal to the

reciprocal of the detection probability:

$$W = \left[\exp(-L_{MIN}/\lambda) - \exp(-D/\lambda)\right]^{-1},$$

where L_{MIN} is 0.75 cm, D is the distance to the edge of the acceptance volume, and λ is the mean decay length for the K^o_S in question. All results presented in this paper are obtained from events selected and weighted according to this procedure. Over the momentum interval 4 to 12 GeV/c, the average value of W for the accepted events is 1.19.

3. Results

3.1 Cross Section for $K^o_L p \to K^o_S \pi^+ \pi^- p$

The cross section for reaction (1) between threshold and 12 GeV/c is given in table 1 and shown as the upper points in fig. 2. The cross section has been corrected for the neutral decay mode of the K^o_S as well as for scanning biases and losses due to decays outside the active scanning volume (see sect. 2). The errors shown include both the uncertainties in event statistics and the uncertainties in the K^o_L momentum distribution as given by the error bars in fig. 1. The absolute scale for the cross section is determined by studying K^o_L beam decays in the bubble chamber. This overall normalization has a systematic uncertainty of $\leq 15\%$ as estimated by the procedures discussed in sect. 2.

The cross section for reaction (1) reaches a maximum near 3.5 GeV/c, and decreases above 5 GeV/c approximately as $P^{-1.2}_{BEAM}$. This falloff is steeper than that observed for the reactions $K^+ p \to K^+ \pi^+ \pi^- p$ and $K^- p \to K^- \pi^+ \pi^- p$ which have momentum dependences proportional to $P^{-0.59}_{BEAM}$ and $P^{-0.32}_{BEAM}$ respectively.[14] This difference can probably be attributed to proton diffraction dissociation which is forbidden for reaction (1) by the requirement of charge conjugation in the t-channel. Proton diffraction dissociation can occur, however, in the reactions $K^{\pm} p \to K^{\pm} \pi^+ \pi^- p$ and in the unobserved reaction $K^o_L p \to K^o_L \pi^+ \pi^- p$.

3.2 $K^o_S\pi^+\pi^-$ Mass Spectrum

The $K^o_S\pi^+\pi^-$ mass spectrum is shown in fig. 3 for four different P_{BEAM} regions and in fig. 4 for the entire P_{BEAM} interval 4 to 12 GeV/c. In all energy regions the data are characterized by a broad enhancement at the lower end of the spectrum. The peripheral nature of the enhancement as well as the importance of the $\Delta^{++}(1236)$ reflection is illustrated by the lower histograms in figs. 3 and 4 where the cuts $|t'| \equiv |t - t_{min}| < 0.5$ GeV^2 and $M(p\pi^+) > 1.34$ GeV have been made. These cuts increase the size of the Q signal with respect to the background in all four energy regions and the shape of the enhancement thus obtained appears to be independent of energy. However, we note that the $\Delta^{++}(1236)$ reflection changes from a large effect below ~5 GeV/c to a minor effect above ~8 GeV/c. Appropriate corrections for this problem will be made in subsequent discussions in order to proceed with our analysis of the Q meson.

The dashed histogram in fig. 4 shows the $K\pi\pi$ mass distribution for events having the additional requirement that at least one $K\pi$ mass combination be in the interval 0.86 to 0.92 GeV. The percentage of events satisfying this narrow K* selection is approximately constant as a function of $K\pi\pi$ mass below 1.5 GeV and is also found to be independent of beam momentum.

3.3 Definition of "Q Region" and Separation of $Q^o p$ and $\bar{Q}^o p$ events

For our analysis we define the "Q region" as those events satisfying the following selections:

(a) $1.1 < M(K\pi\pi) < 1.5$ GeV,

(b) $M(p\pi^+) > 1.34$ GeV, and

(c) $|t'| < 0.5$ GeV^2.

These selections have been consistently imposed for all energies. When suitable corrections are made the results obtained are insensitive to the cuts (b) and (c), except for determining the Q cross section at momenta below ~ 5 GeV/c, as discussed in sect. 3.6.

The Q^o and $\bar{Q}^o$ events are then separated by selecting subsamples of $K^{*+}\pi^-p$ and $K^{*-}\pi^+p$, respectively, from the "Q region". The K* selection is 0.86 to 0.92 GeV and is illustrated in fig. 5 where we have plotted the $K^o_S\pi^-$ and $K^o_S\pi^+$ mass distributions for the events in the Q region. The lower histograms are obtained when the opposing K* reflection is removed. The events selected as $\bar{Q}^o \to K^{*-}\pi^+$ or $Q^o \to K^{*+}\pi^-$ then appear as the shaded bins of the lower histograms.

3.4 Treatment of the $\Delta^{++}(1236)$ Reflection and Other Backgrounds in the Q Region

The primary source of background in the Q region is the reflection of the strong $\Delta^{++}(1236)$ signal. The cut, $M(p\pi^+) > 1.34$ GeV, not only removes the $\Delta^{++}(1236)$ reflection but also removes a fraction of the true Q signal, especially at the lower energies. In addition, the $M(p\pi^+)$ selection is not symmetric between the Q^o and $\bar{Q}^o$ states. In order to determine the extent of these effects and to make appropriate corrections we have made Monte Carlo calculations. The simulated events are given the observed properties of the Q meson (the low mass $K\pi\pi$ enhancement, the observed t' distributions, and an s-wave $K^*\pi$ decay with an aligned K* decay) and then are subjected to the $M(p\pi^+)$ cut. On the basis of these calculations we find that the fraction of events in the Q region which survives the $M(p\pi^+)$ selection varies smoothly from $65 \pm 5\%$ at 4 GeV/c to $96 \pm 2\%$ at 12 GeV/c. The correction needed for the ratio of Q^o to $\bar{Q}^o$ events is much smaller and varies only from $8 \pm 4\%$ at 4 GeV/c to $1 \pm 1\%$ at 12 GeV/c.

These corrections are applied to the Q^o and $\bar{Q}^o$ cross sections in this paper. The calculations also indicate that the $M(p\pi^+)$ cut introduces no significant bias in the shapes of the t' distributions or the $K\pi\pi$ mass distributions for the Q data.

Other backgrounds to the Q region are small. The K*(1420) signal, which affects Q^o and $\bar{Q}^o$ equally, is less than 5% of the Q signal as shown by the shaded region in fig. 4. The K*(1420) signal has been estimated from our data on the reactions $K^o_L p \rightarrow K^{\pm}\pi^{\mp}p$ and the known branching ratio[15] for $(K^*(1420) \rightarrow K\pi\pi)/(K^*(1420) \rightarrow K\pi)$. The Y* background, which might be a source of asymmetry between the Q^o and $\bar{Q}^o$ events, has been reduced to an insignificant level by the combination of the narrow K* requirement and the Q mass definition.

3.5 Comparison of $K\pi\pi$ Mass Spectra for Q^o and $\bar{Q}^o$

Several experiments have shown that the shape of the $K\pi\pi$ mass distribution for the Q is not consistent with a single Breit-Wigner centered near 1.3 GeV.[3] Goldhaber[16] has suggested that the existence of two coherent $J^P = 1^+$ states could produce structure in the $K\pi\pi$ mass distribution. From the simple quark model one expects two 1^+ nonets whose neutral nonstrange members have opposite charge conjugation quantum numbers.[17] However, the two physical states, Q_A and Q_B, could in general be mixtures of the pure nonet states,[18] and the resulting $K\pi\pi$ mass spectrum might be very complicated. This model also suggests that differences might be expected between the mass spectra for Q and $\bar{Q}$.

The experimental comparison is shown in fig. 7a where we have superimposed the mass spectra for $K^{*+}\pi^-$ (solid histogram) and $K^{*-}\pi^+$ (dashed histogram) summed over the energy region 4 to 12 GeV/c. The two distributions have the same shape within statistics, although the $K^{*-}\pi^+$ enhancement

appears to be slightly narrower than the $K^{*+}\pi^-$ enhancement. The ratio of $K^{*+}\pi^-$ to $K^{*-}\pi^+$ events is shown in fig. 7b and is observed to be constant across the entire Q mass interval.†

†The data shown in fig. 7 have not been corrected for the effects of the cuts on t' and $M(p\pi^+)$. However, the Monte Carlo calculations indicate that the number of $K^{*+}\pi^-$ events should be raised by a constant 6% relative to $K^{*-}\pi^+$ events across the entire Q region thereby yielding a ratio consistent with unity.

Thus we observe no significant differences between the Q^o and $\bar{Q}^o$ mass spectra in agreement with the results of previous comparisons of $K\pi\pi$ mass spectra.[3,19]

3.6 Q Production Cross Section

Since the Q meson is usually regarded as a diffractively produced state the production cross section is expected to be nearly independent of energy. In fig. 2 and table 2 we present σ_Q, the cross section for neutral Q production, over the interval 3 to 12 GeV/c, defined as:

$$\sigma_Q \equiv \sigma(K_L^o p \to Q^o p) + \sigma(K_L^o p \to \bar{Q}^o p)$$
$$\equiv \frac{1}{2}\sigma(K^o p \to Q^o p) + \frac{1}{2}\sigma(\bar{K}^o p \to \bar{Q}^o p) ,$$

where the Q^o (or $\bar{Q}^o$) decays into $K_S^o\pi^+\pi^-$. The values given for σ_Q have been adjusted for the neutral K_S^o decay mode, but not for other unseen decay modes of the neutral Q (e.g., not for $Q^o \to K_L^o\pi^+\pi^-$, $K^+\pi^-\pi^o$, etc.) The values shown thus represent about 20% of the total neutral Q production cross section in $K_L^o p$ interactions.†† The cross section has been calculated from the events in the

††The exact fraction is $(4-\alpha)/18$ when all possible $K^*\pi$ and $K\rho$ decay modes are considered, where α is the branching fraction $K\rho/(K\rho + K^*\pi)$.

Q region (defined in sect. 3.3). Corrections have been made for the $\Delta^{++}(1236)$ cut (see sect. 3.4) and in addition for events with short recoil protons or with $|t - t_{min}| > 0.5$ GeV^2.

The values for σ_Q show a gradual rise over the region 3 to 5 GeV/c followed by a gradual falloff above 5 GeV/c. A fit to the parameterization $\sigma_Q \propto P_{BEAM}^{-n}$ above 5 GeV/c yields $n = 0.59 \pm 0.16$, a value which is in good agreement with those obtained for the processes[20,21] $K^+p \rightarrow Q^+p$ ($n = 0.58 \pm 0.15$) and $\pi^-p \rightarrow A_1^-p$ ($n = 0.42 \pm 0.11$) at comparable energies. The shape of σ_Q below 5 GeV/c disagrees with the result found by ref. 20) for the reaction $K^+p \rightarrow Q^+p$. This disagreement emphasizes the difficulty of studying the Q meson at low energy.†

---

†For low energies we find that the t' distribution flattens out for large t' values. This effect accounts for about half of the disagreement since we choose a cut-off, $|t'| < 0.5$ GeV^2, whereas ref. 20) impose no t' cutoff. We suspect that the remainder of the disagreement is due to inherent differences in the final states studied.

It is also interesting to compare the results for σ_Q to Kp elastic scattering. Between 5 and 15 GeV/c, the K^+p and K^-p elastic cross sections fall off gradually with exponents $n = 0.09 \pm 0.03$ and $n = 0.39 \pm 0.04$, respectively.[14] We note in addition that the elastic cross sections are approximately four times larger than the Q production cross sections when all decay modes are included.

3.7 Ratio of $\sigma(Q^0p)/\sigma(\bar{Q}^0p)$

The energy dependence of the ratio $\sigma(Q^0p)/\sigma(\bar{Q}^0p)$ is important in understanding the Q production mechanisms. The equal components of K^0 and $\bar{K}^0$ in the K_L^0 beam allow this comparison to be made over the entire energy region

free from problems of relative normalization between the strangeness states. In fig. 7 we show the experimental values for $\sigma(Q^o p)/\sigma(\bar{Q}^o p)$ calculated from the ratios of observed Q^o and $\bar{Q}^o$ events in the Q region.

We find that $\sigma(Q^o p)/\sigma(\bar{Q}^o p)$ is consistent with a constant value, 0.99 ± 0.08, over the momentum range 4 to 12 GeV/c. The 8% uncertainty includes the statistical uncertainty (7%) and our estimate of the maximum uncertainty introduced by the Δ^{++} correction (4%). This result is similar to the case of elastic Kp scattering where the ratio $\sigma(K^+ p)/\sigma(K^- p)$ is approximately unity above 4 GeV/c.[14] We note that a previous comparison of $Q^+ p$ and $Q^- p$ production cross sections (measured in separate experiments) has suggested that the ratio $\sigma(Q^+ p)/\sigma(Q^- p)$ is greater than one.[22] Such a ratio is incompatible with the observation of the present experiment.

3.8 Differential Cross Sections for Q^o and $\bar{Q}^o$.

Comparisons of $K^+ p$ and $K^- p$ elastic differential cross sections have revealed a crossover at $-t \sim 0.2$ GeV^2. This behavior is explained by the addition of a Regge contribution to the dominant Pomeron term. The similarities between diffraction dissociation and elastic scattering therefore suggest that the crossover effect may also occur in Q production.

The $Q^o p$ and $\bar{Q}^o p$ differential cross sections are shown in fig. 8 and in table 3. The data have been plotted as a function of $t' \equiv t - t_{min}$. Both the Q^o and $\bar{Q}^o$ differential cross sections are well described by single exponentials with no apparent turnover in the forward direction, and with a clear crossover for $-t' \sim 0.15$ GeV^2. To obtain a quantitative determination of the crossover position these distributions have been fitted to single exponentials in the region $0.02 < |t'| < 0.5$ GeV^2. The resulting slope parameter values are 5.9 ± 0.5 and 9.7 ± 0.7 GeV^{-2} for $Q^o p$ and $\bar{Q}^o p$ respectively. The crossover position is

$-t' = 0.13 \pm 0.03$ GeV^2, where the error consists of nearly equal contributions from the uncertainties in the slope parameters and the uncertainty in the ratio $\sigma(Q^o p)/\sigma(\bar{Q}^o p)$.

The differential cross section for Q^o and $\bar{Q}^o$ production therefore are qualitatively similar to those for $K^{\pm}p$ elastic scattering. In the momentum region 5 to 10 GeV/c the K^+p and K^-p elastic differential cross sections have slopes of ~ 5.5 and ~ 7.5 GeV^{-2} respectively,[23] and a crossover at $-t \sim 0.2$ GeV^2. In analogy to elastic scattering we interpret the crossover in Q production as evidence that Regge exchange, in addition to Pomeron exchange, occurs in Q production. The implications of this interpretation are discussed in detail in sect. 4.1.

We have also investigated the dependence of the differential cross section slopes on incident momentum by fitting the $Q^o p$ and $\bar{Q}^o p$ distributions to single exponentials in four momentum intervals between 4 and 12 GeV/c. The results of these fits are shown in fig. 9 and are summarized in table 4. The slope for $\bar{Q}^o p$ is greater than that for $Q^o p$ for all energies. The slopes for both Q^o and $\bar{Q}^o$ are consistent with their average values (dashed lines in fig. 9) over the entire region. On the other hand, $K^{\pm}p$ elastic scattering data would suggest the shrinkage of the $Q^o p$ slopes indicated by the solid curve (derived in sect. 4.1). Unfortunately, the uncertainties are too large to permit a definitive test of the expected shrinkage.

For all momenta from 4 to 12 GeV/c we find that the ratio $\sigma(Q^o p)/\sigma(\bar{Q}^o p)$ is unity and that the slope for $\bar{Q}^o$ is greater than the slope for Q^o. These two observations imply that the crossover must occur at all momenta in this interval.

We observe an interesting dependence of the differential cross section slopes on the $K\pi\pi$ mass for both strangeness states. The results are presented in fig. 10 and table 5. Both the Q^o and $\bar{Q}^o$ slopes are observed to decrease rapidly as a function of $K\pi\pi$ mass with the $\bar{Q}^o$ slope remaining larger than the Q^o slope for all values of $K\pi\pi$ mass. Mass dependences of the slope parameter have been previously observed in charged Q production[1f, 1g, 24, 25] and in other inelastic production channels.[26-29] Various interpretations of this effect have been given,[30-32] and it seems clear that this behavior could not be produced if the Q region consisted of a single resonant state. In sect. 4.2 we further discuss the dependence of the slopes on $K\pi\pi$ mass, and investigate whether a Reggeized Deck model can explain the observed behavior.

3.9 Density Matrix Elements

It has recently been observed that s-channel helicity is approximately conserved[33] in "elastic" scattering, for example $\pi p \to \pi p$ (ref. 34) and $\gamma p \to \rho p$ (ref. 35). On the other hand, diffraction-dissociation data, where the Pomeron is also thought to dominate, are not consistent with s-channel helicity conservation at the meson vertex, but instead suggest approximate t-channel helicity conservation.[2d, 20, 21, 36] The differences in the differential cross sections for Q^o and $\bar{Q}^o$ production make the comparison of the density matrix elements for Q^o and $\bar{Q}^o$ mesons of particular interest for the present data.

The density matrix elements for the Q and $\bar{Q}$ data, in the momentum interval 4 to 12 GeV/c are shown in fig. 11 and tabulated in table 4 for both Gottfried-Jackson and helicity frames. In this analysis we have assumed that the spin-parity of the Q region is $J^P = 1^+$.[1, 2] The density matrix elements have been evaluated using the method of moments with the normal to the $K\pi\pi$ decay plane

as the analyser. The angular variables defining the $K\pi\pi$ system are then the polar coordinates, α and β, of the normal to the decay plane and a third angle γ that specifies the azimuthal orientation of the three momenta in the decay plane.[37]

We have not imposed the $M(p\pi^+)$ cut of sect. 3.3 for the analysis of the density matrix elements. Rather the selection $\underset{\sim}{\pi}^+ \cdot \underset{\sim}{p} < 0$ has been made, where $\underset{\sim}{\pi}^+$ and $\underset{\sim}{p}$ are the three momenta of the π^+ and recoil proton in the $K\pi\pi$ rest frame. This selection effectively removes the $\Delta^{++}(1236)$ contamination. The range of γ is then limited to π instead of the full 2π radians, but the determination of the Q density matrix elements is unaffected. This result follows from the restrictions provided by parity conservation for decays into three pseudoscalar mesons.[38]

Conservation of t-channel helicity is the statement that $\rho_{00} = 1$ and $\rho_{1-1} = \mathrm{Re}\rho_{10} = 0$ in the Gottfried-Jackson or t-channel frame. The solid curves in fig. 11 show the predictions of t-channel helicity conservation as seen in the helicity or s-channel frame. The band of values in the helicity frame corresponds to our range of beam momentum, 4 to 12 GeV/c.

We find that both the Q^o and the $\bar{Q}^o$ data are in agreement with t-channel helicity conservation. The matrix elements for $\bar{Q}^o$ clearly disagree with s-channel helicity conservation, whereas the disagreement for Q^o is not as strong. The systematic difference between the values for ρ_{00} in the helicity frame is an interesting, although not statistically compelling effect.

Various speculations on the density matrix results are possible. For example, the presence of Regge exchanges in Q production could cause s-channel helicity to be violated even if it is conserved by Pomeron exchange.[39] An alternative possibility is that Pomeron exchange conserves t-channel helicity at vertices where there is a spin change.[40] In this case it is possible

in Q production for t-channel helicity to be conserved at the meson vertex simultaneously with s-channel helicity at the baryon vertex.

4. Q Meson Production Mechanisms

In this section we interpret the experimental results for $Kp \to Qp$ and $\bar{K}p \to \bar{Q}p$ in terms of the underlying production mechanisms. First (sect. 4.1) we discuss the implications of the observed crossover of the Qp and $\bar{Q}p$ differential cross sections by analogy to elastic scattering. The relative strengths of Pomeron and Regge exchanges in Q production are then compared to those for elastic scattering, and conjectures are made concerning the expected magnitude of nondiffractive Q production and the expected differences between the reactions $K^{\pm}p \to Q^{\pm}p$. Next (sect. 4.2) we turn to a discussion of the predictions of a Reggeized Deck Model. Such models have been reasonably successful in reproducing many aspects of diffraction dissociation processes. In this discussion we investigate whether such a model can describe the energy dependence of the Q meson production as well as the behavior of the differential cross sections for both Qp and $\bar{Q}p$.

4.1 Interpretation of the Crossover of Qp and $\bar{Q}p$ Differential Cross Sections

Both elastic scattering and diffraction dissociation are generally believed to be dominated by Pomeron exchange since they have large cross sections which are nearly independent of energy. However, the crossover of the differential cross sections for these reactions is evidence that Regge exchanges are also important. This point has also been discussed recently by Cohen-Tannoudji et al.[39] based in part on a preliminary report of the crossover effect observed in the present experiment.

A procedure to extract the Regge contribution to elastic scattering has been developed recently by Davier and Harari.[8] For $K^{o}p$ and $\bar{K}^{o}p$ elastic

scattering the amplitudes† are:

$$A(K^o p \to K^o p) = A_P + A_T - A_V$$
$$A(\bar{K}^o p \to \bar{K}^o p) = A_P + A_T + A_V \,, \tag{2}$$

---

†The amplitudes for $K^o p$ and $\bar{K}^o p$ are directly related by isospin to those for $K^+ n$ and $K^- n$, respectively. However, in order to relate these amplitudes to the $K^+ p$ and $K^- p$ amplitudes one needs to use SU(3) f/d ratios in addition to isospin. This remark also applies to the relations between neutral and charged Q production.

---

where A_V (A_T) represents a combination of Reggeized $\rho^o + \omega^o$ (A_2^o and f^o) exchanges and A_P represents Pomeron exchange. It is assumed that the dominant Pomeron term is purely imaginary and conserves s-channel helicity. With these assumptions one may write (ignoring terms quadratic in the Regge amplitudes):

$$\frac{d\sigma}{dt}(K^o p) \simeq |A_P|^2 + 2A_P\,(\mathrm{Im}\,A_T - \mathrm{Im}\,A_V)$$
$$\frac{d\sigma}{dt}(\bar{K}^o p) \simeq |A_P|^2 + 2A_P\,(\mathrm{Im}\,A_T + \mathrm{Im}\,A_V) \,,$$

where the Regge amplitudes are now restricted to be nonflip s-channel amplitudes. For the exotic $K^o p$ reaction the net Regge amplitude is limited by duality[41,42] to be predominantly real. Therefore it is a good approximation to equate $\frac{d\sigma}{dt}(K^o p)$ to $|A_P|^2$. Values for $\mathrm{Im}\,A_V$ then can be extracted directly from the data as follows:

$$2\,\mathrm{Im}\,A_V \simeq \frac{\frac{d\sigma}{dt}(\bar{K}^o p) - \frac{d\sigma}{dt}(K^o p)}{2\left[\frac{d\sigma}{dt}(K^o p)\right]^{1/2}} \,.$$

Diffraction dissociation is a more complicated process than elastic scattering. Six independent amplitudes contribute to Q meson production ($J^P = 1^+$ state) compared with only two for elastic scattering. Nevertheless, the Davier-Harari analysis can be extended to Q meson production by averaging over the allowed helicity amplitudes. In what follows we denote the change of helicity at the baryon (meson) vertex by λ (μ). For each helicity amplitude equation (2) also applies when $Q^o p$ ($\bar{Q}^o p$) is substituted for $K^o p$ ($\bar{K}^o p$) in the final state.† Following the above procedure, we find:

$$\frac{d\sigma}{dt'}(Q^o p) \simeq \sum_{\lambda\mu} \left[|\mathcal{A}_P^{\lambda\mu}|^2 + 2\mathcal{A}_P^{\lambda\mu} \left(\mathrm{Im}\,\mathcal{A}_T^{\lambda\mu} - \mathrm{Im}\,\mathcal{A}_V^{\lambda\mu} \right) \right]$$

$$\frac{d\sigma}{dt'}(\bar{Q}^o p) \simeq \sum_{\lambda\mu} \left[|\mathcal{A}_P^{\lambda\mu}| + 2\mathcal{A}_P^{\lambda\mu} \left(\mathrm{Im}\,\mathcal{A}_T^{\lambda\mu} + \mathrm{Im}\,\mathcal{A}_V^{\lambda\mu} \right) \right]$$

---

†Throughout this discussion we will assume that the Q belongs to a 1^+ nonet whose neutral nonstrange members have positive charge conjugation ($J^{PC} = 1^{++}$). The existence of a $J^{PC} = 1^{+-}$ state in the Q region would complicate the simple formalism which we use but would not significantly modify our conclusions.

The difference in the differential cross sections is then given by the interference term:

$$\frac{d\sigma}{dt'}(\bar{Q}^o p) - \frac{d\sigma}{dt'}(Q^o p) = \sum_{\lambda\mu} 4\mathcal{A}_P^{\lambda\mu}\, \mathrm{Im}\,\mathcal{A}_V^{\lambda\mu}. \qquad (3)$$

If we assume that the Pomeron amplitude is smoothly varying in t', then the imaginary part of the Regge term, averaged over helicities, must change sign at the position of the crossover of the differential cross sections. It is also interesting to note that for the momentum range 4 to 12 GeV/c the integral

over t' of the right hand side of (3) must be approximately zero since the cross sections for $Q^o p$ and $\bar{Q}^o p$ are equal over this momentum range.

To obtain an estimate of the Regge contribution, we define the average:

$$\langle \mathrm{Im}\, R(t') \rangle \equiv \frac{\sum_{\lambda\mu} 2 \mathscr{A}_P^{\lambda\mu} \, \mathrm{Im}\, \mathscr{A}_V^{\lambda\mu}}{\left[\sum_{\lambda\mu} |\mathscr{A}_P^{\lambda\mu}|^2 \right]^{1/2}}$$

$$\simeq \frac{\frac{d\sigma}{dt'}(\bar{Q}^o p) - \frac{d\sigma}{dt'}(Q^o p)}{2\left[\frac{d\sigma}{dt'}(Q^o p)\right]^{1/2}} . \qquad (4)$$

Experimental values for $\langle \mathrm{Im}\, R(t') \rangle$ have been evaluated from the differential cross sections and are shown in fig. 12. The solid curve is taken from the exponential fits to the differential cross sections shown in fig. 8:

$$\langle \mathrm{Im}\, R(t') \rangle = \frac{1.36 \exp(9.7t') - 0.83 \exp(5.9t')}{2\left[0.83 \exp(5.9t')\right]^{1/2}} \, \mathrm{mb}^{1/2} \, \mathrm{GeV}^{-1} .$$

For elastic scattering the behavior of $\langle \mathrm{Im}\, R \rangle$ has been interpreted in terms of a geometrical picture[43,44] in which the Regge exchanges contribute mainly to peripheral impact parameters. Using this picture, Davier and Harari have proposed a parameterization for the nonflip amplitude which is proportional to the zeroth order Bessel function, $J_0(r\sqrt{-t'})$, where r is the "interaction radius" in impact parameter space. Over the t' range studied, this parameterization provides a good representation (dashed curve in fig. 12) for the Q meson data:

$$\langle \mathrm{Im}\, R(t') \rangle = 0.3 \exp(0.7t') \, J_0(6.5\sqrt{-t'}) \, \mathrm{mb}^{1/2} \, \mathrm{GeV}^{-1} .$$

However, the factor 6.5 GeV^{-1} (1.3 fm) should not be taken literally as the interaction radius since several helicity amplitudes probably are important for $< \mathrm{Im}\, R(t') >$.

An indication of the relative importance of the amplitudes contributing to $< \mathrm{Im}\, R >$ can be found by examining the general features of the experimental data. Since no turnover of the forward differential cross section is observed in Q production, the amplitudes with nonzero values for the net helicity flip, $\lambda + \mu$, must be small. In addition, t-channel helicity is nearly conserved at the meson vertex (see sect. 3.9). These two facts therefore suggest that an important component in $< \mathrm{Im}\, R >$ is the t-channel helicity nonflip amplitude. Of course, the relative importance of the allowed helicity amplitudes would be clarified by polarization information at the baryon vertex.

In the above paragraphs we have implicitly treated Q production as a sum of single exchange diagrams involving both Pomeron and Regge exchanges. We note, however, that the present analysis is still applicable if Q production is assumed instead to proceed through multiparticle exchange diagrams (such as shown in fig. 13) that include Regge in addition to Pomeron exchange at the baryon vertex. Thus the present discussion does not depend on the "resonance" versus "kinematic enhancement" interpretation of the Q region.

Several further observations may now be made on the basis of the preceding analysis.

(1) Strength of the Pomeron term in Q production relative to elastic scattering

For our average beam momentum of ~ 7 GeV/c the differential cross section at $t' = 0$ for $K^o p \to Q^o p$ is 3.9 ± 0.8 mb/GeV^2 when corrections are made for all unobserved decay modes of the Q^o. For comparison the forward

differential cross section for K^+p elastic scattering[45] at 7 GeV/c is 20 ± 4 mb/GeV^2. At $t' = 0$ the density matrix elements (see sect. 3.9) imply that $\lambda = \mu = 0$. We then find:

$$\left| \frac{\mathscr{A}_P^{00}(0)}{A_P(0)} \right| = \left[\frac{\frac{d\sigma}{dt'}(Q^o p)}{\frac{d\sigma}{dt'}(K^+ p)} \right]^{1/2}_{t'=0} = 0.4 \pm 0.1 \ .$$

Thus the Pomeron amplitude is approximately half as large for Q production as for Kp elastic scattering.

(2) Strength of the Regge term in Q production relative to elastic and inelastic scattering

Noting again that $\lambda = \mu = 0$ for $t' = 0$, we have from equation (4):

$$2 \, \mathrm{Im} \mathscr{A}_V^{00}(0) \simeq \left[\frac{\frac{d\sigma}{dt'}(\bar{Q}^o p) - \frac{d\sigma}{dt'}(Q^o p)}{2 \cdot \frac{d\sigma}{dt'}(Q^o p)} \right]^{1/2}_{t'=0} .$$

The corresponding Regge amplitude in $K^o p$ and $\bar{K}^o p$ (or equivalently, $K^+ n$ and $K^- n$) elastic scattering can be determined directly from the inelastic reaction $K_L^o p \to K_S^o p$, where

$$A(K_L^o p \to K_S^o p) = \frac{1}{2}\left[A(K^o p) - A(\bar{K}^o p) \right]$$

$$= -A_V \ .$$

The ratio of real to imaginary parts of $A_V(0)$ is known to be near unity.[46-48] Therefore we have:

$$\frac{d\sigma}{dt}(K_L^o p \to K_S^o p)_{t=0} \simeq 2 \left[\mathrm{Im} \, A_V(0) \right]^2 \ .$$

The ratio of Regge amplitudes is then:

$$\left|\frac{\mathrm{Im}\,\mathcal{A}_V^{00}(0)}{\mathrm{Im}\,A_V(0)}\right| \simeq \left|\frac{\frac{d\sigma}{dt'}(\bar{Q}^o p) - \frac{d\sigma}{dt'}(Q^o p)}{\left[8\frac{d\sigma}{dt'}(Q^o p)\,\frac{d\sigma}{dt}(K_S^o p)\right]^{1/2}}\right| .$$

Correcting for unobserved decay modes of the Q^o meson and using experimental values[46] for the forward differential cross section for $K_L^o p \to K_S^o p$, we find for ~ 7 GeV/c:

$$\left|\frac{\mathrm{Im}\,\mathcal{A}_V^{00}(0)}{\mathrm{Im}\,A_V(0)}\right| = 0.8 \pm 0.3 \quad .$$

Therefore, approximately equal Regge contributions are found for the reaction $K_L^o p \to K_S^o p$ (and consequently for $K^o p$ and $\bar{K}^o p$ elastic scattering) and for neutral Q meson production. We note in addition that other inelastic reactions such as $\pi^- p \to \pi^o n$ (charge exchange)[49,50] or $\pi N \to \Sigma K$ (hypercharge exchange)[51,52] have differential cross sections at $t=0$ similar to that for $K_L^o p \to K_S^o p$ (therefore similar Regge strengths) over the momentum interval 5 - 10 GeV/c.

(3) Strength of the Regge contribution as a function of $K\pi\pi$ mass in the Q region

Although we have established the existence of Regge exchanges in the Q mass region, we have not determined the shape of the $K\pi\pi$ mass spectrum which would be produced by the Regge amplitude in the absence of Pomeron exchange. The strength of the Regge amplitude as a function of $K\pi\pi$ mass can be deduced from the following ratio:

$$\left|\frac{\mathrm{Im}\,\mathcal{A}_V^{00}(0)}{\mathcal{A}_P^{00}(0)}\right| \simeq \left\{\frac{\frac{d\sigma}{dt'}(\bar{Q}^o p) - \frac{d\sigma}{dt'}(Q^o p)}{4\frac{d\sigma}{dt'}(Q^o p)}\right\}_{t'=0} . \qquad (5)$$

This ratio is consistent with a constant value of 0.17 over the entire Q mass region. Therefore we conclude that the Regge contribution by itself will produce a $K\pi\pi$ mass enhancement with roughly the same shape as that for the Pomeron term alone.

(4) Nondiffractive Q production

We find $\int dt' \left| < \mathrm{Im}\, R(t') > \right|^2 \sim 30\ \mu b$ when corrections are made for all decay modes of the neutral Q meson. Therefore we expect that Q production in charge or hypercharge exchange reactions will have cross sections on the order of 30 μb in the momentum range 5 - 10 GeV/c. It is interesting to note that enhancements above phase space having cross sections of this order are seen in the reactions $K^- p \rightarrow (\bar{K}\pi\pi)^0 n$ at 10 GeV/c (ref. 25) as well as in $\pi^- p \rightarrow (K\pi\pi)^0 \Lambda$ at 6 GeV/c (ref. 53), although in the latter experiment the $K\pi\pi$ enhancement appears to be quite narrow.

(5) Shrinkage of the forward slopes for Q production

The analogy to elastic scattering suggests that the $Q^0 p$ differential cross section should exhibit shrinkage. The extent of the expected shrinkage can be estimated from the experimental slopes for $K^{\pm} p$ elastic scattering. From eq. (5), we obtain:

$$\frac{\bar{B} - B}{B} \simeq 4 \left| \frac{\mathrm{Im}\, \mathcal{A}_V^{00}(0)}{\mathcal{A}_P^{00}(0)} \right| ,$$

where B ($\bar{B}$) is the exponential slope parameter for $Q^0 p$ ($\bar{Q}^0 p$) and where the ratio $\sigma(Q^0 p)/\sigma(\bar{Q}^0 p)$ is taken to be unity for all energies (see fig. 7). A similar relation applies for $K^{\pm} p$ elastic scattering. From the present analysis we find $\left| \mathrm{Im}\, \mathcal{A}_V^{00}(0)/\mathcal{A}_P^{00}(0) \right| \simeq 0.17$ whereas Davier and Harari find a value

$\simeq 0.19$ in their analysis of $K^{\pm}p$ elastic scattering at 5 GeV/c.† It follows therefore that

$$\frac{\bar{B} - B}{B} \simeq \frac{b^- - b^+}{b^+} ,$$

where b^+ and b^- are the slope parameters for K^+p and K^-p elastic scattering respectively.

---

†As noted in the footnote to eq. (2), the SU(3) f/d ratios at the baryon vertex are important when relating K^0p or $\bar{K}^0p$ results to K^+p or K^-p results. Thus it is somewhat fortuitous that the ratios of vector to Pomeron strengths for neutral Q production and $K^{\pm}p$ elastic scattering are approximately equal.

The solid curve in fig. 9 shows the prediction for B versus energy assuming that $\bar{B} = 10$ GeV^{-2} for all energies, where the experimental values[23] for b^+ and b^- have been used. The data are compatible with the expected shrinkage. However, more precise measurements are needed to test the small variation of B over this energy range.

(6) Crossover in the differential cross sections for $K^{\pm}p \rightarrow Q^{\pm}p$

From the results of the present experiment, we expect that the crossover phenomenon should also be seen in the reactions $K^{\pm}p \rightarrow Q^{\pm}p$. Published values of the exponential slope parameters suggest that the crossover does in fact occur. Specific examples for slope parameters are: for Q^-p, 8.5 ± 1.0 GeV^{-2} at 10 GeV/c (ref. 25) and 11 ± 2 GeV^{-2} at 12.6 GeV/c (ref. 2f); for Q^+p, 6.7 ± 0.5 GeV^{-2} at 10 GeV/c (ref. 1f) and 7.4 ± 0.3 GeV^{-2} at 12 GeV/c (ref. 1g). Detailed comparisons of Q^+p and Q^-p based on presently published results are difficult, however, because of systematic differences between Q meson definitions and absolute normalizations for the various experiments. Of particular

interest with regard to the present discussion would be careful comparisons of the slope parameters for Q^+p and Q^-p above $\sim$ 10 GeV/c to see whether (and at what rate) the slopes become equal. If the present analogy to elastic scattering is correct, we expect the slopes to become equal as the Regge contribution diminishes with increasing energy.

4.2 Comparison with a Reggeized Deck Model

In contrast to the preceding analysis a more conventional approach has been to study Q production in terms of the Deck effect, when one of the components of the dissociated beam particle scatters diffractively off the target. Several versions of such a model have been applied to the data at a wide range of incident energies.[1,2] In general, reasonable agreement has been obtained with the shape of the Q mass enhancement and with the s-wave character of the $K\pi\pi$ decay.

Our data are particularly well suited to investigate two aspects of the Deck model which have not received much attention: namely, the energy dependence of the cross section for $Kp \rightarrow Qp$ and the behavior of the differential cross sections for Q and $\bar{Q}$ production.

For our comparisons we consider a Reggeized Deck model (RDM) based on diagrams A and B in fig. 13. The general form of the amplitude, M, for both diagrams is[11]

$$M \propto \beta(t_2)\left(\frac{S_2}{S_0}\right)^{\alpha(t_2)} S_1^{\alpha_P} e^{\lambda t_1/2} ,$$

where S_i and t_i are the subenergies and momentum transfers squared indicated in fig. 13. Linear Regge trajectories are used for the $\alpha(t_2)$ whereas the Pomeron is assumed to be a fixed pole, $\alpha_P = 1$. The parameter λ is the

forward slope of π or K* elastic scattering. The vertex function, $\beta(t_2)$, is given by the signature factor and the Reggeized propagator with no additional form factor.

For our calculations we have chosen the functional forms and parameters shown in table 7. The $K^{*\pm}p$ elastic scattering slopes in diagram B have been set equal to those for $K^{\pm}p$ elastic scattering. Diagrams A and B have been added coherently in proportion to the total cross sections (σ) for $\pi^{\mp}p$ and $K^{\pm}p$. In order to make the comparison over the widest possible region of phase space the only restriction made is that the mass squared of the proton and the bachelor pion ($S_{p\pi}$) be greater than 2 GeV^2.† The model calculated according

---

†This cut limits one to the region where Pomeron exchange contributes strongly to diagram A. There are essentially no events in the data or in the model for $|t_{KK^*}| > 1.5$ GeV^2, $|t_{K\pi}| > 1.5$ GeV^2, or $S_{K^*p} < 4$ GeV^2, therefore we have not made further restrictions on these variables.

---

to this prescription is in good qualitative agreement with the shape and decay distribution of the low mass $K^*\pi$ enhancement in our data (not shown) even though a fit of the parameters was not performed. We have tried several modifications, such as varying the relative normalization of diagrams A and B, adding the diagrams incoherently, and replacing the S_i by the cosh ξ_i functions of Bali, Chew, and Pignotti.[10] However, neither these modifications nor more restrictive t_2 and S_1 cuts affected the following analysis.

The energy dependence of the RDM cross section is compared to the data for $K^0_L p \rightarrow Qp$ in fig. 14. The definition of the Q region is the same as that in fig. 2 with the additional restriction on $S_{p\pi}$ as discussed above. The predictions of diagrams A and B of the RDM are shown by the dotted and dashed curves

respectively, while the solid curve shows their coherent sum. The curves are averages of the predictions for the two strangeness states $K^{*+}\pi^-p$ and $K^{*-}\pi^+p$. The coherent sum has been normalized to the data at 7 GeV/c assuming that the Q decays completely into $K^*\pi$.

It is seen from fig. 14 that both diagrams as well as their coherent sum have a flat energy dependence above 6 GeV/c, in contrast to the data, which fall off with increasing energy. This is evidence that Regge exchange may be required in addition to the Pomeron exchange in the RDM, in agreement with the conclusion of sect. 4.1. Alternatively, this effect can be achieved by using a Pomeron trajectory with intercept smaller than one, since the energy dependence of a multi-Regge model is determined by the leading trajectory.[10)]

The RDM predictions for the slope of the $K^{*+}\pi^-p$ and $K^{*-}\pi^+p$ differential cross sections are compared to the data as a function of the $K^*\pi$ mass in fig. 15. Diagram A (dotted curve) predicts a strong dependence of the slopes on the $K^*\pi$ mass but fails to give a steeper slope for $K^{*-}\pi^+$ than for $K^{*+}\pi^-$. On the other hand, diagram B (dashed curve) provides the observed difference in the slope magnitudes, but not the dependence on the $K^*\pi$ mass. The coherent sum of A and B (solid curve) also fails to describe the data adequately.

The slope predictions of diagrams A and B have simple qualitative explanations. Diagram B reproduces the observed slope difference because in the calculation the slope for $K^{*-}p$ elastic scattering is assumed to be steeper than that for $K^{*+}p$. In contrast, diagram A predicts a slope difference in the wrong direction since π^-p elastic scattering has a slightly steeper slope than that for π^+p. Diagram A reproduces the rapid fall of the slope with increasing $K^*\pi$ mass because of the closeness of the pion pole to the physical region. The strong peaking of t_2 caused by the pion propagator is reflected into the t_1

distribution since these two variables are strongly correlated for small $K^*\pi$ mass. On the other hand, diagram B does not give a strong mass dependence to the slope since the K^* propagator is a slowly varying function of t_2.

Thus the present parameterization for the RDM fails to describe the behavior of the forward slopes for Q production when both strangeness states are considered together. Furthermore, the constant cross section predicted in the model is not in agreement with the data. Although it may be possible to improve the agreement by modifying the model, it appears inescapable that more than one RDM diagram will be required to describe the data.

5. Summary and Conclusions

We have presented experimental results on the reactions $K^0p \rightarrow Q^0p$ and $\bar{K}^0p \rightarrow \bar{Q}^0p$ from 4 to 12 GeV/c with special emphasis on a detailed comparison of the production characteristics of the two strangeness states. The principal features of the data are:

a. The production cross sections above 5 GeV/c obey a power law, $\sigma_Q \sim P_{BEAM}^{-n}$, with $n = 0.59 \pm 0.16$.

b. The ratio $\sigma(Q^0p)/\sigma(\bar{Q}^0p)$ is consistent with a constant value, 0.99 ± 0.08, over the entire momentum interval.

c. The differential cross sections for Q^0p and $\bar{Q}^0p$ have exponential slope parameters of 5.9 ± 0.5 GeV^{-2} and 9.7 ± 0.7 GeV^{-2} respectively and exhibit a crossover for $-t' = 0.13 \pm 0.03$ GeV^2.

d. The slope parameters for Q^0 and $\bar{Q}^0$ both diminish as the $K^*\pi$ mass increases, with the $K^{*-}\pi^+$ component (strangeness = -1) remaining larger than the $K^{*+}\pi^-$ component (strangeness = +1) for all $K^*\pi$ masses.

e. The density matrix elements for both Q^0 and $\bar{Q}^0$ are in agreement with t-channel helicity conservation; s-channel helicity conservation is violated strongly by the $\bar{Q}^0$ data but not as strongly by the Q^0 data.

f. No significant difference is observed between the Q^0 and $\bar{Q}^0$ mass spectra.

The crossover of the Q^0 and $\bar{Q}^0$ differential cross sections is an important observation of this study and we find that a simple model employing a coherent sum of Regge and Pomeron exchanges can account for this effect. The ratio of Regge to Pomeron is found to be constant as a function of $K\pi\pi$ mass over the Q region, and we estimate that nondiffractive Q production (charge exchange or hypercharge exchange) occurs with a cross section $\sim 30\ \mu b$ in the momentum range 5 - 10 GeV/c. The dependence of the exponential slope parameter on $K\pi\pi$ mass remains a problem, however, and points out the complicated nature of the Q enhancement. We have made calculations with a Reggeized Deck Model and find that such models, as presently formulated, cannot account for the observed behavior of the differential cross sections or the energy dependence of the Q production cross section.

Acknowledgements

We thank F. Gilman, R. Cashmore, and M. Davier for interesting discussions. We are grateful for the assistance given to us by R. Watt and the crew of the SLAC 40-inch bubble chamber and by J. Brown and the scanning and measuring staff at SLAC. We also thank D. Johnson for his help with data reduction.

References

1a. B. C. Shen, I. Butterworth, C. Fu, G. Goldhaber, and G. H. Trilling, Phys. Rev. Letters 17 (1966) 726

1b. W. De Baere et al., Bruxelles - CERN Collaboration, Nuovo Cimento 49A (1967) 373

1c P. Antich, R. Carson, C. Y. Chien, B. Cox, D. Denegri, L. Ettlinger, D. Feiock, G. Goodman, R. Mercer, L. Resvanis, R. L. Sekulin, A. Pevsner, and R. Zdanis, Nucl. Phys. B20 (1970) 201

1d. C. Y. Chien, E. I. Malamud, D. J. Mellema, F. D. Rudnick, P. E. Schlein, W. E. Slater, D. H. Stork, H. K. Ticho, and T. G. Trippe, Phys. Letters 29B (1969) 433

1e. G. Alexander, A. Firestone, G. Goldhaber, and D. Lissauer, Nucl. Phys. B13 (1979) 503

1f. K. W. J. Barnham et al., Birmingham - Glasgow - Oxford Collaboration, Nucl. Phys. B25 (1970) 49

1g. P. J. Davis, M. Alston-Garnjost, A. Barbaro-Galtieri, S. M. Flatté, J. H. Friedman, G. R. Lynch, M. S. Rabin, and F. T. Solmitz, LBL-36 (1971), submitted to Phys. Rev.

1h. M. S. Farber, T. Ferbel, P. F. Slattery, and H. Yuta, Phys. Rev. D1 (1970) 78.

2a. J. C. Park, S. Kim, G. Chandler, G. Ascoli, E. L. Goldwasser, and T. P. Wangler, Phys. Rev. Letters 20 (1968) 171

2b. D. C. Colley et al., Birmingham - Glasgow - London - München - Oxford - Rutherford Collaboration, Nuovo Cimento 59A (1969) 519

2c. S. U. Chung, R. L. Eisner, N. F. Bali, and D. Luers, Phys. Rev. 182 (1969) 1443

2d. B. Buschbeck et al., Athen - Democritos - Liverpool - Vienna Collaboration, Nucl. Phys. B35 (1971) 511

2e. J. Bartsch et al., Aachen - Berlin - CERN - London - Vienna Collaboration, Nucl. Phys. B24 (1970) 221

2f. T. Ludlam, J. Sandweiss, and A. J. Slaughter, Phys. Rev. D2 (1970) 1234

3. A. Firestone, Experimental meson spectroscopy, ed. Baltay and Rosenfeld (Columbia University Press, New York, 1970) p. 229

4. U. E. Kruse, Phenomenology in particle physics 1971, ed. Chiu, Fox, and Hay (California Institute of Technology, Pasadena, 1971) p. 27

5. M. L. Good and W. D. Walker, Phys. Rev. 120 (1960) 1857

6. R. T. Deck, Phys. Rev. Letters 13 (1964) 169

7. G. W. Brandenburg, W. B. Johnson, D.W.G.S. Leith, J. S. Loos, G. J. Luste, J.A.J. Matthews, K. Moriyasu, W. M. Smart, F. C. Winkelmann, and R. J. Yamartino, Phys. Rev. Letters 28 (1972) 932

8. M. Davier and H. Harari, Phys. Letters 35B (1971) 239

9. H. A. Gordon, K. W. Lai, and F. E. Paige, Comparison of elastic $(\bar{p}p, pp)$, (K^-p, K^+p), and (π^-p, π^+p) scattering at 8 and 16 GeV/c, BNL preprint (1971)

10. N. F. Bali, G. F. Chew, and A. Pignotti, Phys. Rev. Letters 19 (1967) 614

11. E. L. Berger, Phys. Rev. 166 (1968) 1525

12. A. D. Brody, W. B. Johnson, D.W.G.S. Leith, G. Loew, J. S. Loos, G. Luste, R. Miller, K. Moriyasu, B. C. Shen, W. M. Smart, and R. Yamartino, Phys. Rev. Letters 22 (1969) 966

13. G. W. Brandenburg et al., to be published

14. E. Flaminio, J. D. Hansen, D.R.O. Morrison, and N. Tovey, CERN/HERA 70-4 (1970); CERN/HERA 70-6 (1970)

15. M. Aguilar-Benitez, D. Bassano, R. L. Eisner, J. B. Kinson, N. P. Samios, and V. E. Barnes, Phys. Rev. Letters 25 (1970) 1362

16. G. Goldhaber, Phys. Rev. Letters 19 (1967) 976

17. R. H. Dalitz, Symmetries and the strong interactions, Proc. of the Thirteenth International Conference on High Energy Physics, Berkeley, 1966 (University of California Press, Berkeley, 1967)

18. G. L. Kane and H. S. Mani, Phys. Rev. 171 (1968) 1533

19. A. Firestone, G. Goldhaber, D. Lissauer, and G. H. Trilling, Phys. Rev. D5 (1972) 505

20. F. Grard, P. Herquet, R. Windmolders, H. H. Bingham, L. Eisenstein, Y. Goldschmidt-Clermont, V. P. Henri, and J. Quinquard, Lett. Nuovo Cimento 2 (1971) 305

21. G. Ascoli et al., Phys. Rev. Letters 26 (1971) 929

22. T. Ferbel, Diffraction production of bosons, Proc. of the Joint Japanese-U. S. Seminar on Elementary Particle Physics with Bubble Chamber Detectors, Stanford, 1971, Report No. SLAC-144 (1972)

23. T. Lasinski, R. Levi Setti, B. Schwarzschild, and P. Ukleja, Nucl. Phys. B37 (1972) 1

24. G. Bassompierre et al., Bruxelles-CERN Collaboration, Nucl. Phys. B9 (1969) 295

25. D.R.O. Morrison, Review of quasi two-body reactions, CERN/D.Ph II/Phys. 71-10 (1970), to be published in Proc. of the Fifteenth International Conference on High Energy Physics, Kiev, 1970

26. Y. Eisenberg, B. Haber, E. E. Ronat, A. Shapira, Y. Stahl, G. Yekutieli, J. Ballam, G. B. Chadwick, M. M. Menke, P. Seyboth, S. Dagan, and A. Levy, Phys. Rev. D5 (1972) 15

27. T. F. Johnson, A. W. Key, J. D. Prentice, T. S. Yoon, A. F. Garfinkel, R. Morse, B. Y. Oh, and W. D. Walker, Nucl. Phys. B24 (1970) 253

28. W. Kittel, S. Ratti, and L. Van Hove, Nucl. Phys. B30 (1971) 333

29. K. Boesebeck et al., Aachen - Berlin - Bonn - CERN - Cracow Collaboration, Nucl. Phys. B28 (1971) 381

30. B. Y. Oh and W. D. Walker, Phys. Letters 28B (1968) 564

31. Y. Eisenberg and L. Lyons, The slope of the momentum transfer distribution, Weizmann Institute preprint (1970)

32. H. Satz, Phys. Letters 32B (1970) 380

33. F. J. Gilman, J. Pumplin, A. Schwimmer, and L. Stodolsky, Phys. Letters 31B (1970) 387

34. V. Barger and F. Halzen, Phys. Rev. Letters 28 (1972) 194

35. J. Ballam et al., Phys. Rev. Letters 24 (1970) 960

36. J. V. Beaupré et al., Aachen - Berlin - Bonn - CERN - Cracow - Heidelberg - London - Vienna Collaboration, Phys. Letters 34B (1971) 160

37. J. D. Jackson, Les Houches summer school in theoretical physics, ed. DeWitt and Jacob (Gordon and Breach, New York, 1965) p. 326

38. S. Berman and M. Jacob, Phys. Rev. 139 (1965) B1023

39. G. Cohen-Tannoudji, G. L. Kane, and C. Quigg, Nucl. Phys. B37 (1972) 77

40. L. Stodolsky, Phys. Rev. Letters 18 (1967) 973

41. H. Harari, Phys. Rev. Letters 22 (1969) 562

42. J. L. Rosner, Phys. Rev. Letters 22 (1969) 689

43. A. Dar, Proceedings of the Third International Conference on High Energy Physics and Nuclear Structure, Columbia University, 1969

44. H. Harari, Ann. Phys. 63 (1971) 432

45. K. J. Foley, S. J. Lindenbaum, W. A. Love, S. Ozaki, J. J. Russel, and L.C.L. Yuan, Phys. Rev. Letters 11 (1963) 503

46. A. D. Brody, W. B. Johnson, B. Kehoe, D.W.G.S. Leith, J. S. Loos, G. J. Luste, K. Moriyasu, B. S. Shen, W. M. Smart, F. C. Winkelmann, and R. J. Yamartino, Phys. Rev. Letters 26 (1971) 1050

47. C. D. Buchanan, D. J. Drickey, F. D. Rudnick, P. F. Shepard, D. H. Stork, H. K. Ticho, C. Y. Chien, B. Cox. L. Ettinger, L. Resvanis, R. A. Zdanis, E. Dally, E. Seppi, and P. Innocenti, Phys. Letters 37B (1971) 213

48. P. Darriulat, C. Grosso, M. Holder, J. Pilcher, E. Radermacher, C. Rubbia, M. Scire, A. Stande, and K. Tittel, Phys. Letters 33B (1970) 433

49. A. V. Stirling, P. Sonderegger, J. Kirz, P. Falk-Vairant, O. Guisan, C. Bruneton, P. Borgeaud, M. Yvert, J. P. Guillaud, C. Caverzasio, and B. Amblard, Phys. Rev. Letters 14 (1965) 763; Phys. Letters 20 (1966) 75

50. M. A. Wahlig and I. Manelli, Phys. Rev. 168 (1968) 1515

51. P. Kalbaci, C. W. Akerlof, P. K. Caldwell, C. T. Coffin, D. I. Meyer, P. Schmueser, and K. C. Stanfield, Phys. Rev. Letters 27 (1971) 74

52. A. Bashian, G. Finocchiaro, M. L. Good, P. D. Grannis, O. Guisan, J. Kirz, Y. Y. Lee, R. Pittman, G. C. Fischer, and D. D. Reeder, Phys. Rev. D4 (1971) 2667

53. D. J. Crennell, G. R. Kalbfleisch, K. W. Lai, J. M. Scarr, and T. G. Shumann, Phys. Rev. Letters 19 (1967) 44

Table 1

Cross Section for $K_L^o p \rightarrow K_S^o \pi^+ \pi^- p$

P_{BEAM}(GeV/c)	EVENTS[a]	$\sigma(\mu b)$[b]
1.50 - 1.75	49	179±30
1.75 - 2.00	115	315±34
2.00 - 2.25	211	465±39
2.25 - 2.50	289	539±37
2.50 - 2.75	331	547±35
2.75 - 3.00	422	634±36
3.0 - 3.5	978	674±26
3.5 - 4.0	1042	678±26
4.0 - 4.5	964	622±24
4.5 - 5.0	991	655±25
5.0 - 5.5	862	604±25
5.5 - 6.0	743	568±25
6.0 - 7.0	1266	577±22
7.0 - 8.0	769	464±23
8.0 - 9.0	451	381±25
9.0 -10.0	239	299±28
10.0 -11.0	146	300±38
11.0 -12.0	69	246±51

[a] Corrected for losses of K_S^o charged decays due to finite chamber.

[b] Includes neutral decay mode of K_S^o. Quoted error combines the uncertanties in event statistics with the relative uncertainties in beam flux across the momentum region. The overall systematic error in cross section is 15%.

Table 2

Q Cross Section. $K_L^o p \rightarrow Qp$, $Q \rightarrow K_S^o \pi^+ \pi^-$.

P_{BEAM}(GeV/c)	$\sigma(\mu b)$[a]
3.0 - 3.5	118±25
3.5 - 4.0	138±22
4.0 - 4.5	144±16
4.5 - 5.0	151±15
5.0 - 5.5	165±15
5.5 - 6.0	162±14
6.0 - 7.0	171±13
7.0 - 8.0	149±14
8.0 - 9.0	132±14
9.0 - 10.0	123±16
10.0 - 12.0	99±18

[a]Includes neutral decay mode of K_S^o. The quoted error combines uncertainties in event statistics, in beam flux, and in the procedure used to remove the $\Delta^{++}(1236)$ background. See text for the definition of the Q region.

Table 3

Differential Cross Sections for $K^o p \to Q^o p$ and $\bar{K}^o p \to \bar{Q}^o p$. [a]

$\lvert t - t_{min} \rvert$ (GeV^2)	$\frac{d\sigma}{dt'}$ ($\mu b/GeV^2$)	
	$Q^o p$ [b]	$\bar{Q}^o p$ [b]
0.02 - 0.05	656±98	1071±120
0.05 - 0.10	419±59	661± 73
0.10 - 0.15	463±65	354± 53
0.15 - 0.20	289±49	188± 40
0.20 - 0.25	264±48	161± 34
0.25 - 0.30	140±33	124± 31
0.30 - 0.35	125±33	69± 23
0.35 - 0.45	50±15	32± 12
0.45 - 0.60	53±12	11± 5

[a] Averaged over 4 to 12 GeV/c.

[b] Includes only decays of neutral Q into $K^o_S \pi^+ \pi^-$, corrected for the neutral K^o_S decay mode; the Q region is defined in the text.

Table 4

Slopes of Q^o and $\bar{Q}^o$ Differential Cross Sections

as a Function of Beam Momentum.

P_{BEAM}(GeV/c)	$B(Q^o)^a$ (GeV^{-2})	$B(\bar{Q}^o)^a$ (GeV^{-2})
4 - 5	6.4±1.0	8.2±1.1
5 - 6	5.2±1.0	9.9±1.2
6 - 8	6.4±1.0	9.0±1.2
8 - 12	5.4±1.0	11.3±1.6

[a] Events are selected in the momentum transfer interval $0.02 < |t - t_{min}| < 0.5$ GeV^2, and in the mass interval $1.1 < M(K^*\pi) < 1.5$ GeV.

Table 5

Slopes of Q^o and $\bar{Q}^o$ Differential Cross Sections

as a Function of $K^o_S\pi^+\pi^-$ Mass.

$M(K^o_S\pi^+\pi^-)$ (GeV)	$B(K^{*+}\pi^-)$[a] (GeV^{-2})	$B(K^{*-}\pi^+)$[a] $(GeV)^{-2}$
1.0 - 1.2	8.7±1.1	13.8±1.7
1.2 - 1.3	6.6±1.1	11.6±1.4
1.3 - 1.4	5.5±1.1	8.9±1.1
1.4 - 1.5	3.3±1.0	6.4±1.1
1.5 - 1.75	2.9±1.0	5.4±1.0

[a] Events are selected in the momentum interval 4 to 12 GeV/c and in the momentum transfer interval $0.02 < |t - t_{min}| < 0.5$ GeV^2.

Table 6

Density Matrix Elements for Q^o and $\overline{Q}^o$ Regions.[a]

Reference Frame	$\lvert t - t_{min} \rvert$ (GeV^2)	Q^o			$\overline{Q}^o$		
		ρ_{00}	ρ_{1-1}	$Re\rho_{10}$	ρ_{00}	ρ_{1-1}	$Re\rho_{10}$
Gottfried-Jackson	0.0 - 0.06	1.02±0.11	0.21±0.17	-0.06±0.11	0.88±0.11	-0.11±0.13	0.10±0.07
	0.06 - 0.15	0.87±0.13	-0.44±0.15	-0.05±0.09	0.70±0.13	0.07±0.15	0.16±0.09
	0.15 - 0.40	0.82±0.13	-0.11±0.15	-0.11±0.08	0.89±0.15	0.00±0.17	0.11±0.10
Helicity	0.0 - 0.06	0.92±0.14	0.16±0.17	0.24±0.10	0.71±0.11	-0.20±0.12	0.24±0.08
	0.06 - 0.15	0.80±0.13	-0.48±0.15	0.10±0.08	0.31±0.16	-0.12±0.14	0.29±0.09
	0.15 - 0.40	0.61±0.13	-0.22±0.14	0.24±0.09	0.20±0.19	-0.35±0.14	0.25±0.10

[a] The data are summed over the interval 4 to 12 GeV/c. See text for a discussion of the evaluation technique used.

Table 7

Reggeized Deck Model

	Diagram A (π Exchange)		Diagram B (K* Exchange)	
$\beta(t_2)$	$\frac{e^{-i\pi\alpha}+1}{\sin\pi\alpha}$		$(\alpha+1)\frac{e^{-i\pi\alpha}-1}{\sin\pi\alpha}$	
$\alpha(t_2)$	$t_2 - m_\pi^2$		$t_2 - m_{K^*}^2 + 1$	
α_P	1		1	
S_o	1		1	
	π^-	π^+	K^{*+}	K^{*-}
λ $(GeV)^{-2}$	8.	7.	5.	7.5
σ (mb.)	30.	30.	18.	24.

Figure Captions

1. Shape of the K_L^o beam momentum spectrum.

2. Cross sections for $K_L^o \rightarrow K_S^o\pi^+\pi^-p$ (circles) and $K_L^o p \rightarrow Qp$, $Q \rightarrow K_S^o\pi^+\pi^-$ (squares) where the "Q" is defined in the text. The curves are fits to the form $\sigma \propto P_{BEAM}^{-n}$ with $n = 1.20 \pm 0.12$ (upper curve) and $n = 0.59 \pm 0.16$ (lower curve).

3. Mass distributions for the $K_S^o\pi^+\pi^-$ system.

   (a) $4 < P_{BEAM} < 5$ GeV/c (2028 events),

   (b) $5 < P_{BEAM} < 6$ GeV/c (1640 events),

   (c) $6 < P_{BEAM} < 8$ GeV/c (2077 events),

   (d) $8 < P_{BEAM} < 12$ GeV/c (904 events).

   The upper histograms include all events. The lower histograms include events for which $|t'| < 0.5$ GeV^2 and $M(p\pi^+) > 1.34$ GeV.

4. Mass distribution for the $K_S^o\pi^+\pi^-$ system summed over the entire momentum region $4 < P_{BEAM} < 12$ GeV/c (6649 events). The upper histogram includes all events. The solid subhistogram includes events for which $|t'| < 0.5$ GeV^2 and $M(p\pi^+) > 1.34$ GeV. The dashed histogram is further restricted to events with $K\pi$ masses between 0.86 and 0.92 GeV. The shaded region is our estimate of the K*(1420) signal.

5. Mass distributions for (a) $K_S^o\pi^-$ and (b) $K_S^o\pi^+$ for Q events (see text for definition of the Q). The upper histogram includes all Q events; in the lower histogram the reflections due to the opposing K*(890) band are removed. The shaded region (0.86 to 0.92 GeV) defines the K*(890) events used for our analysis.

6. (a) Comparison of mass distributions for $K^*(890)^+\pi^-$ (solid histogram) and $K^*(890)^-\pi^+$ (dashed histogram). The histograms include events

for which $|t'| < 0.5$ GeV^2 and $M(p\pi^+) > 1.34$ GeV.

(b) Ratio of $K^{*+}(890)\pi^-$ to $K^{*-}(890)\pi^+$ as a function of mass.

7. Ratio $\sigma(K_L^o p \to Q^o p)/\sigma(K_L^o p \to \bar{Q}^o p)$ versus beam momentum. The dashed curve is the averaged ratio (0.99 ± 0.08) over the interval $4 < P_{BEAM} < 12$ GeV/c.

8. Differential cross sections for $K^o p \to Q^o p$ (squares) and $\bar{K}^o p \to \bar{Q}^o p$ (circles) over the momentum range 4 to 12 GeV/c. The scale of the ordinate is determined for neutral Q mesons decaying into $K_S^o \pi^+ \pi^-$. The curves result from the following exponential fits: $\frac{d\sigma}{dt'}(Q^o p) = 0.83 \exp(5.9\, t')$ mb/GeV^2, $\frac{d\sigma}{dt'}(\bar{Q}^o p) = 1.36 \exp(9.7\, t')$ mb/GeV^2.

9. Exponential slope parameter, B, versus P_{BEAM} for $K^o p \to Q^o p$ (squares) and $\bar{K}^o p \to \bar{Q}^o p$ (circles). The average values over the interval $4 < P_{LAB} < 12$ GeV/c are shown as dashed lines and have values 5.9 ± 0.5 GeV^{-2} and 9.7 ± 0.7 GeV^{-2} for $Q^o p$ and $\bar{Q}^o p$ respectively. The solid curve is an estimate of the behavior for $K^o p \to Q^o p$ obtained by a comparison to Kp elastic scattering (see text).

10. Exponential slope parameter, B, averaged over the interval $4 < P_{BEAM} < 12$ GeV/c and plotted versus the mass of the $K^*(890)^+\pi^-$ (squares) and the mass of the $K^*(890)^-\pi^+$ (circles).

11. Density matrix elements for $K^o p \to Q^o p$ (squares) and $\bar{K}^o p \to \bar{Q}^o p$ (circles).
(a) - (c) ρ_{00}, ρ_{1-1}, and $\mathrm{Re}\rho_{10}$ in the Gottfried-Jackson (t-channel) frame,
(d) - (f) ρ_{00}, ρ_{1-1}, and $\mathrm{Re}\rho_{10}$ in the helicity (s-channel) frame.
The curves are calculated assuming t-channel helicity conservation.
The shaded bands indicate the spread expected in the s-channel frame over the momentum interval 4 to 12 GeV/c.

12. Values for $<\mathrm{ImR}>$ determined from the difference between $Q^{o}p$ and $\overline{Q}^{o}p$ differential cross sections. $<\mathrm{ImR}>$ represents the Regge amplitude contributing to Q production (see text). The solid curve is obtained from the exponential fits shown in fig. 8. The dashed curve is obtained using the zeroth order Bessel function parameterization of ref. 8 (see text).

13. Diagrams A (π exchange) and B (K* exchange) for the Reggiezed Deck Model (RDM).

14. RDM predictions for the cross sections for neutral Q production. The data are the same as in fig. 2 with the additional restriction that $S_{p\pi} > 2\ \mathrm{GeV}^2$ (see text). The solid curve is the prediction of the coherent sum of RDM diagrams A and B normalized to the data. The predictions of the individual diagrams A and B are shown by the dotted and dashed curves respectively.

15. RDM predictions for the slopes of the differential cross sections for (a) $K^{*+}\pi^{-}p$ and (b) $K^{*-}\pi^{+}p$ as functions of $K^{*}\pi$ mass. The data are the same as in fig. 10. The RDM curves are defined as in fig. 14.

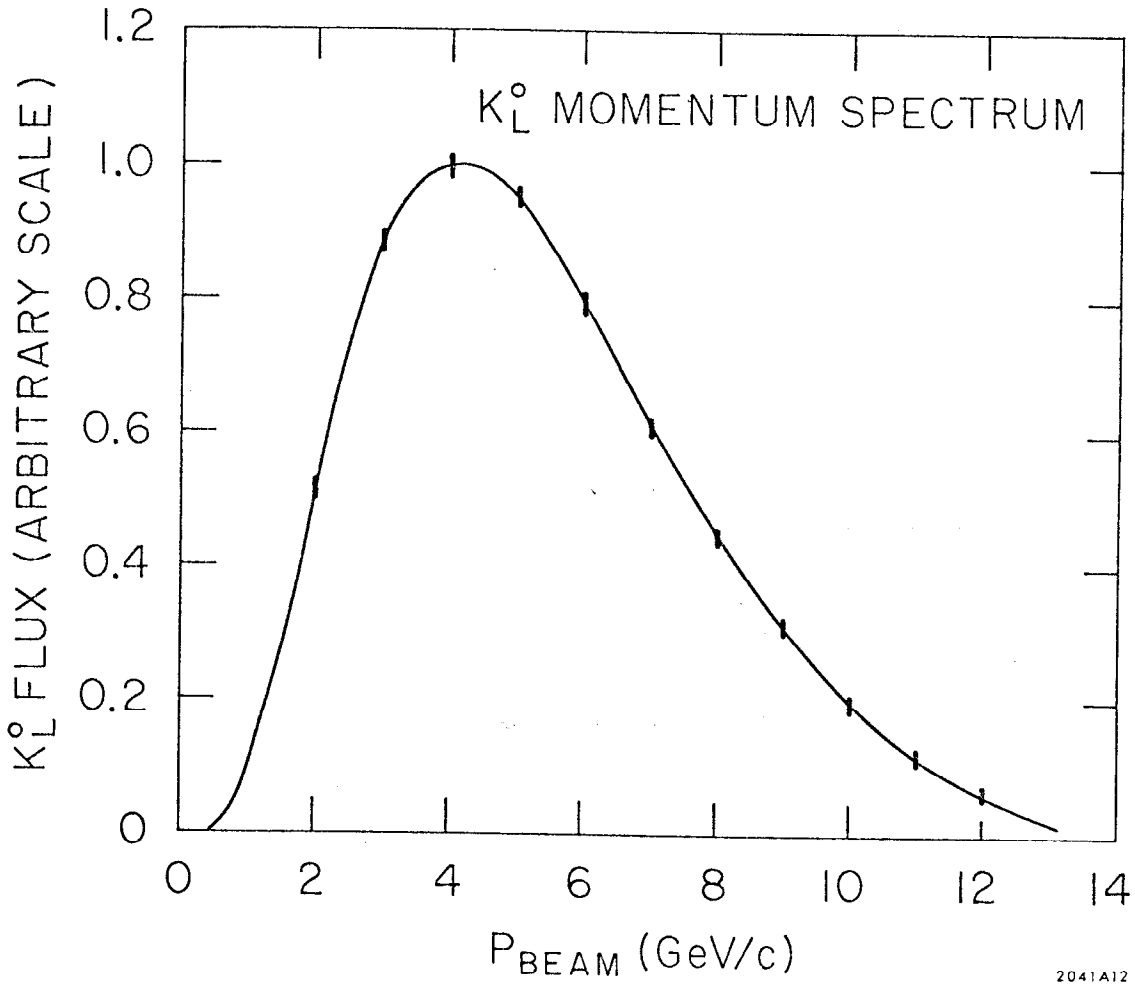
K_L° MOMENTUM SPECTRUM
K_L° FLUX (ARBITRARY SCALE)
1.2
1.0
0.8
0.6
0.4
0.2
0
0
2
4
6
8
10
12
14
P_{BEAM} (GeV/c)
2041A12

Fig. 1

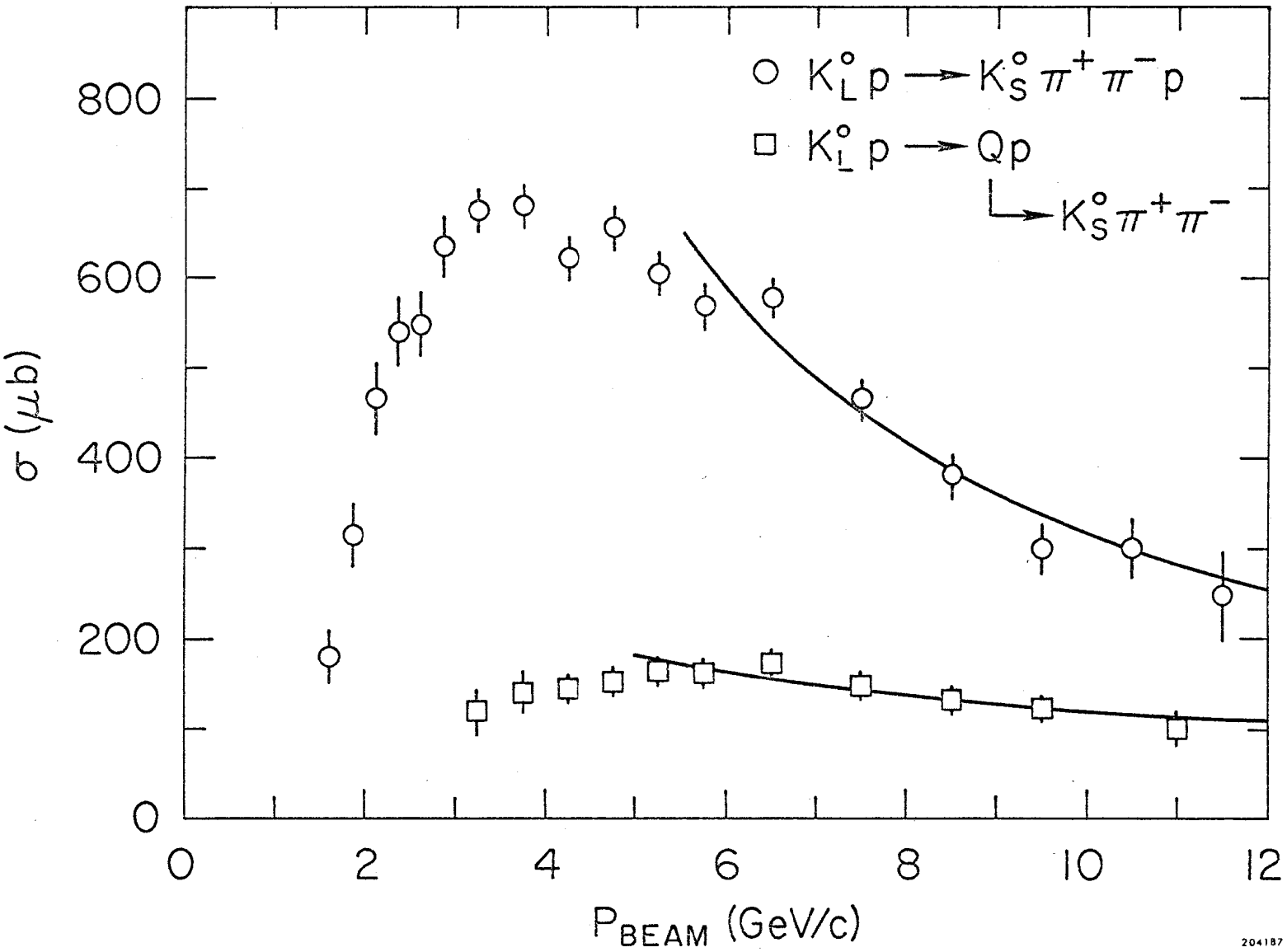
$K_L^0 p \rightarrow K_S^0 \pi^+ \pi^- p$
$K_L^0 p \rightarrow Qp$
$\hookrightarrow K_S^0 \pi^+ \pi^-$
σ (μb)
800
600
400
200
0
0
2
4
6
8
10
12
P_{BEAM} (GeV/c)
204187

Fig. 2

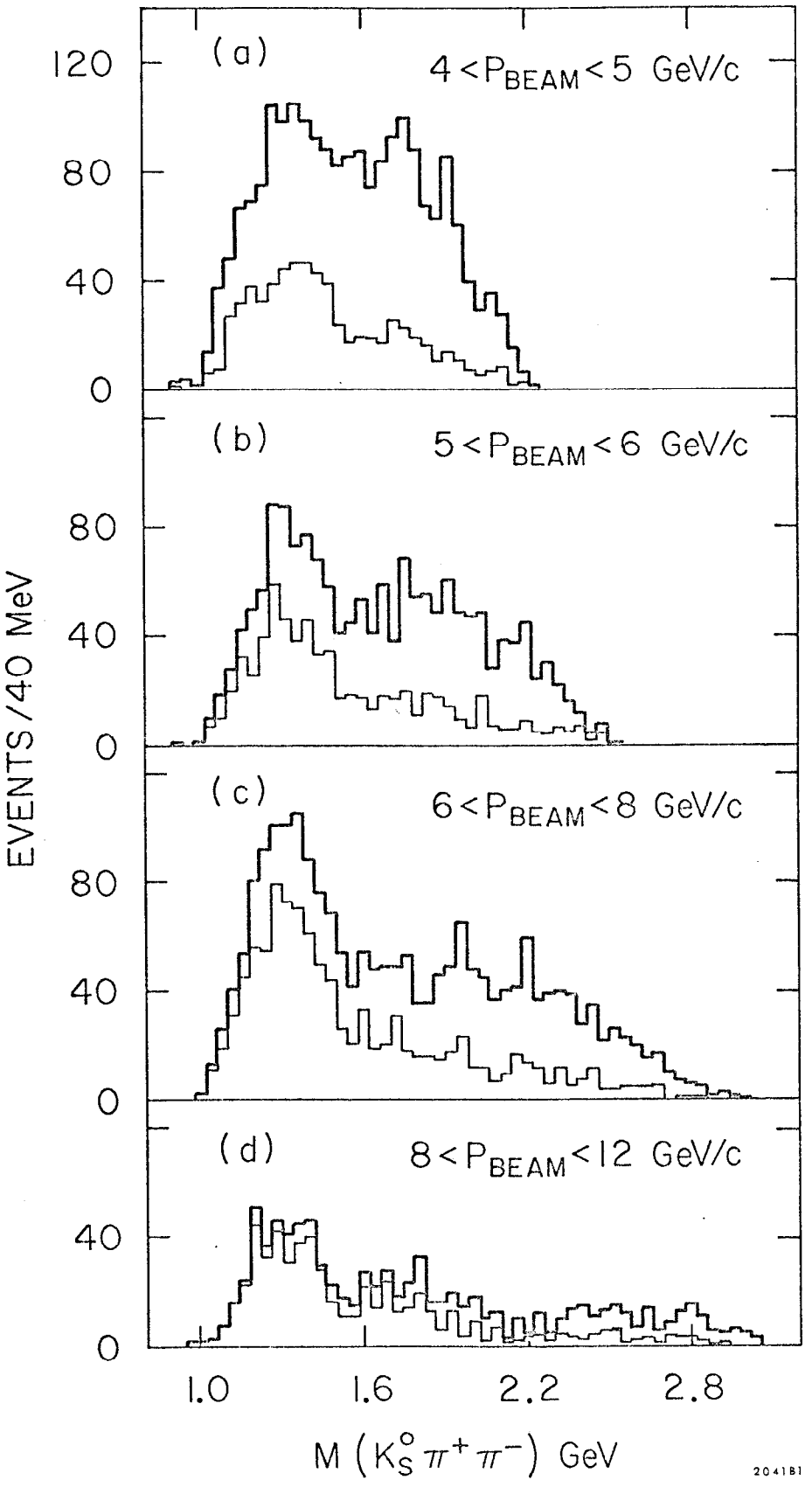
(a)
4<P_BEAM<5 GeV/c
(b)
5<P_BEAM<6 GeV/c
(c)
6<P_BEAM<8 GeV/c
(d)
8<P_BEAM<12 GeV/c
120
80
40
0
EVENTS/40 MeV
1.0
1.6
2.2
2.8
M (K°S π+ π−) GeV
2041B1

Fig. 3

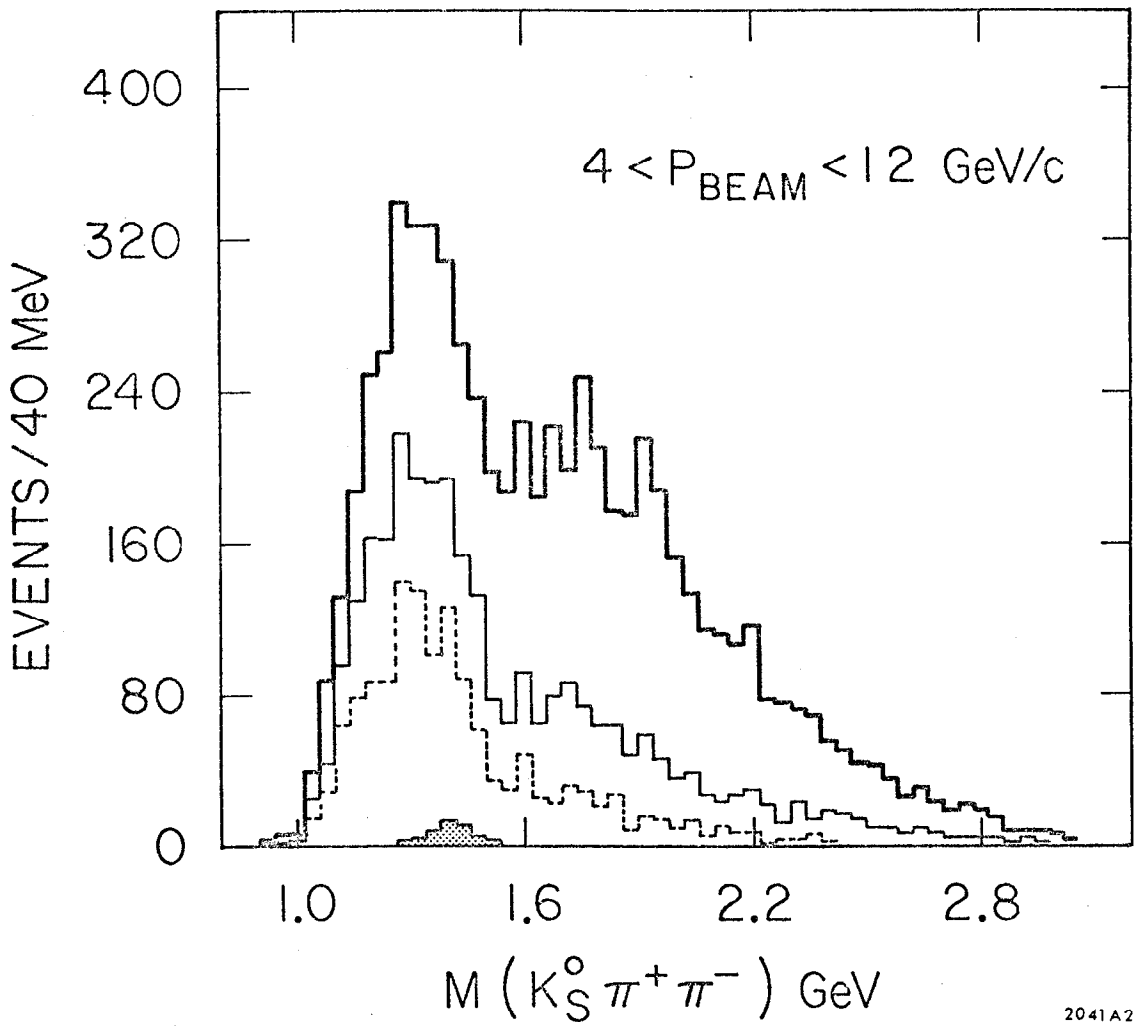
400
320
240
160
80
0
EVENTS/40 MeV
4 < P BEAM < 12 GeV/c
1.0
1.6
2.2
2.8
M (K° S π+ π−) GeV
2041A2

Fig. 4

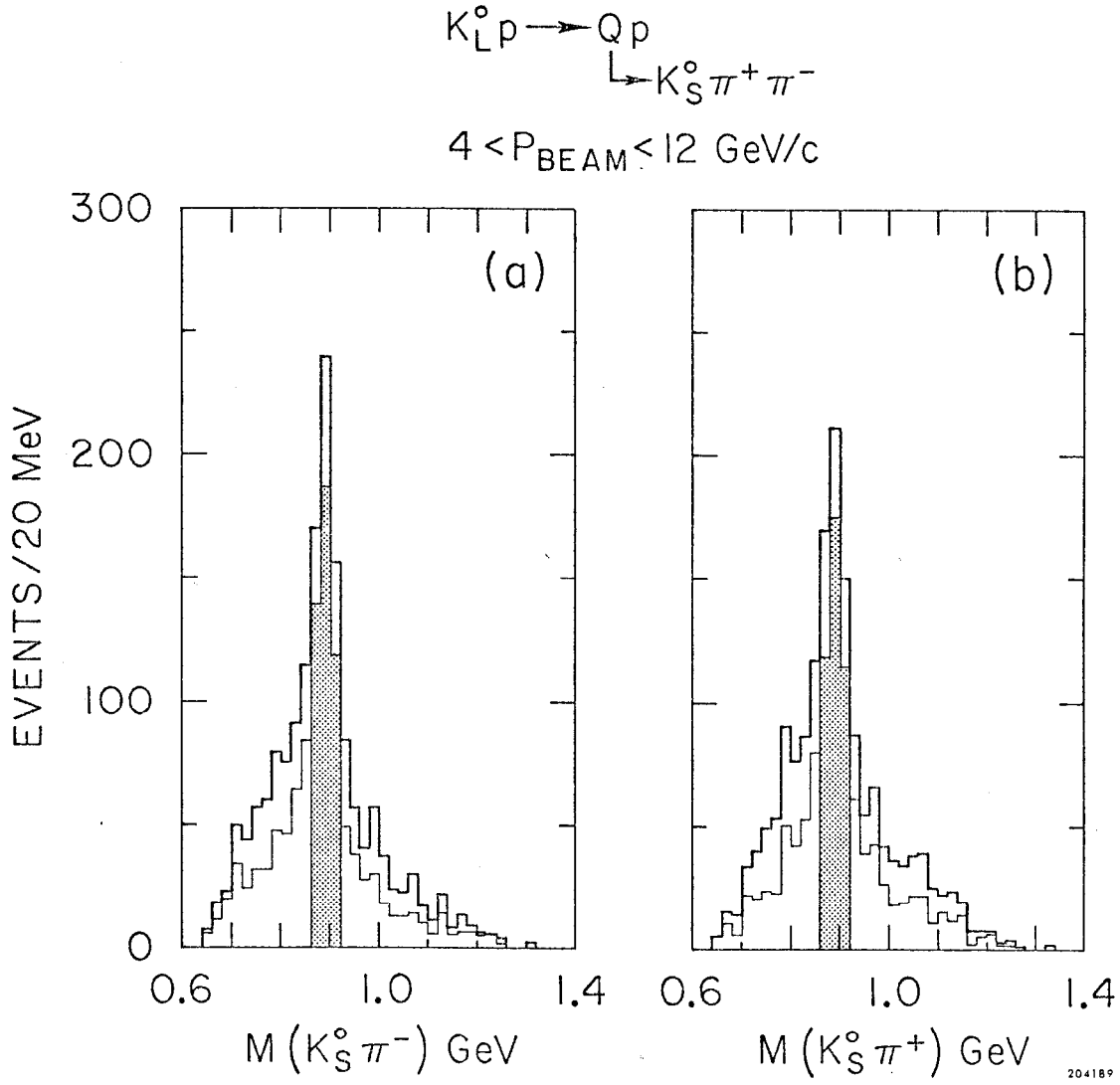
$K^0_L p \rightarrow Q p$
$\hookrightarrow K^0_S \pi^+ \pi^-$
$4 < P_{BEAM} < 12$ GeV/c
300
200
100
0
EVENTS/20 MeV
(a)
(b)
0.6
1.0
1.4
$M(K^0_S \pi^-)$ GeV
$M(K^0_S \pi^+)$ GeV
204189

Fig. 5

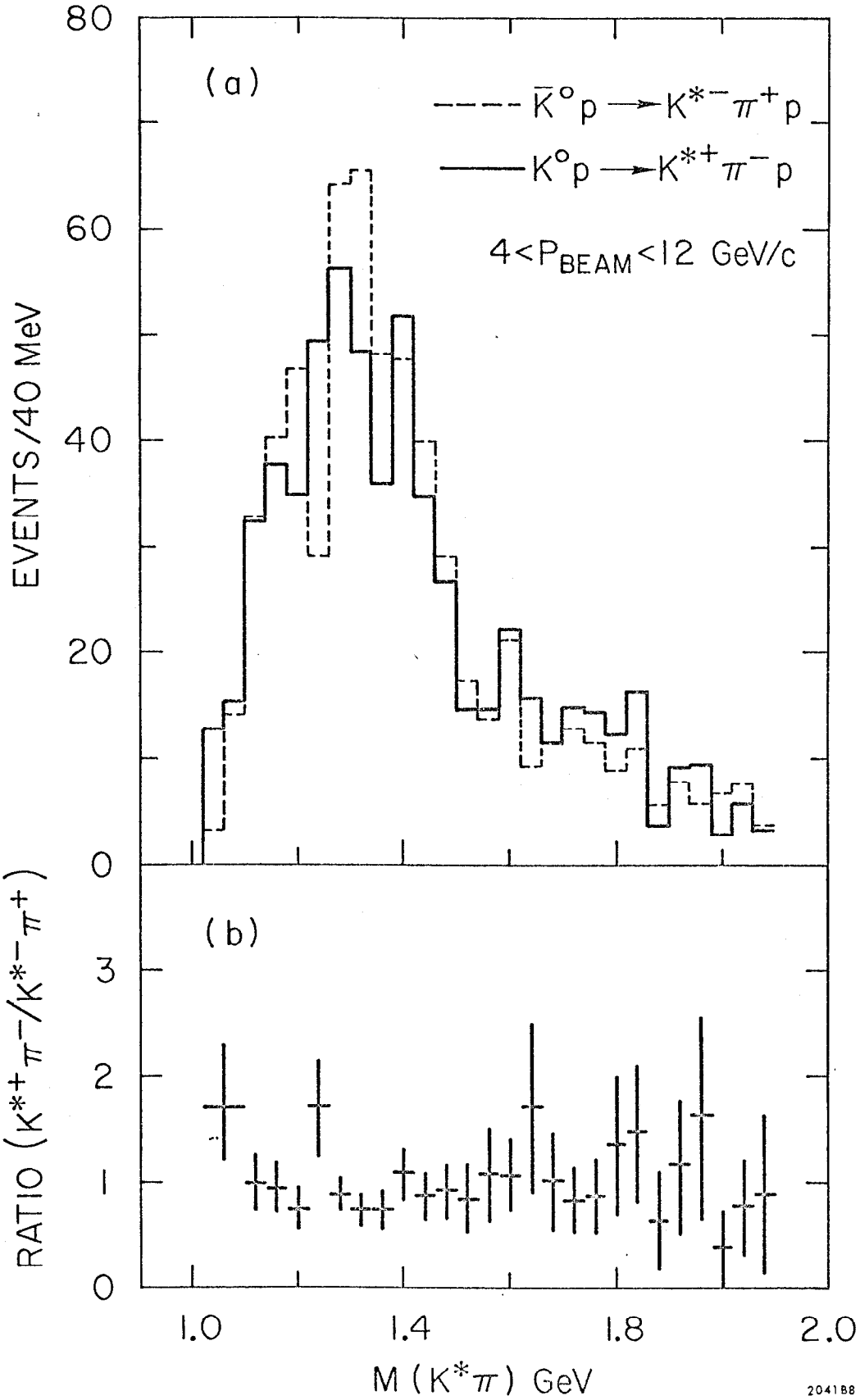
(a)
$\bar{K}^0 p \rightarrow K^{*-}\pi^+ p$
$K^0 p \rightarrow K^{*+}\pi^- p$
$4 < P_{BEAM} < 12$ GeV/c
EVENTS/40 MeV
80
60
40
20
0
(b)
RATIO $(K^{*+}\pi^-/K^{*-}\pi^+)$
3
2
1
0
1.0
1.4
1.8
2.0
M ($K^*\pi$) GeV
2041B8

Fig. 6

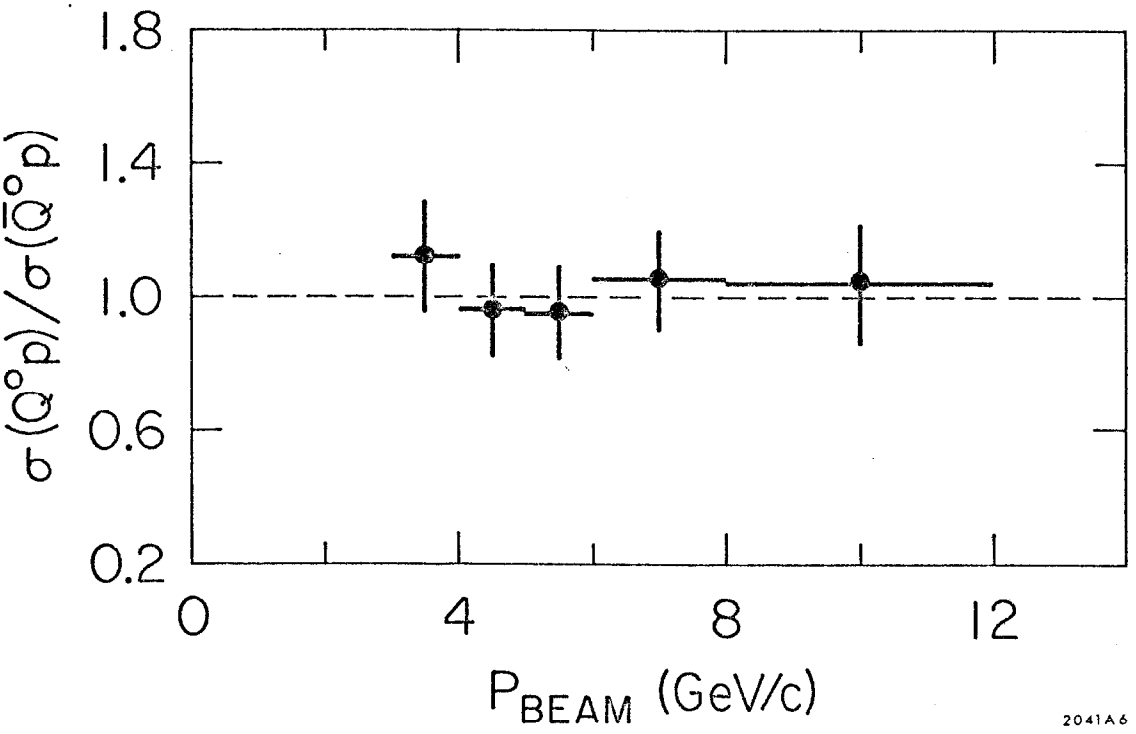

Fig. 7

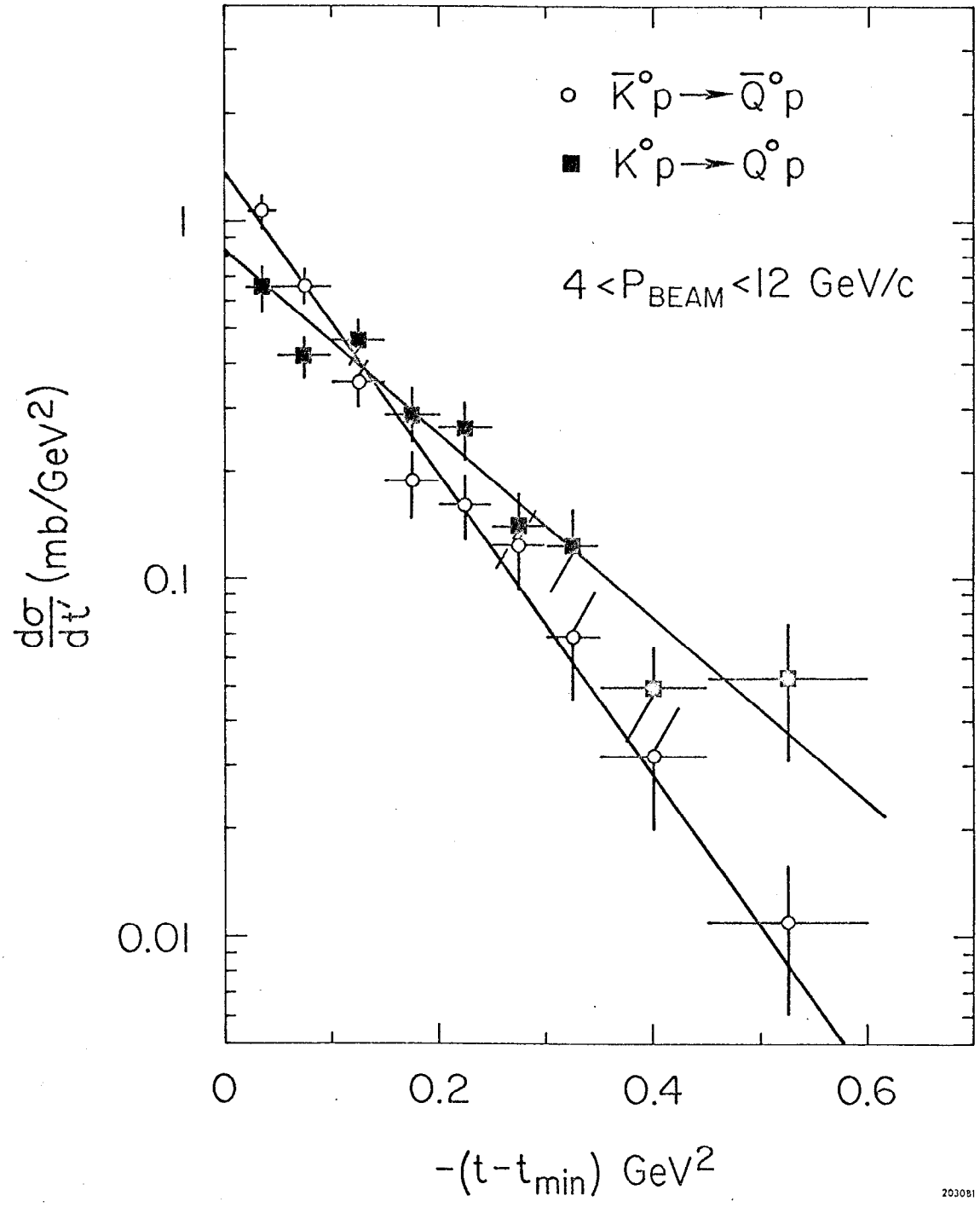
$\bar{K}^0p \rightarrow \bar{Q}^0p$
$K^0p \rightarrow Q^0p$
$4 < P_{BEAM} < 12$ GeV/c
$\frac{d\sigma}{dt'}$ (mb/GeV^2)
1
0.1
0.01
0
0.2
0.4
0.6
$-(t-t_{min})$ GeV^2
203081

Fig. 8

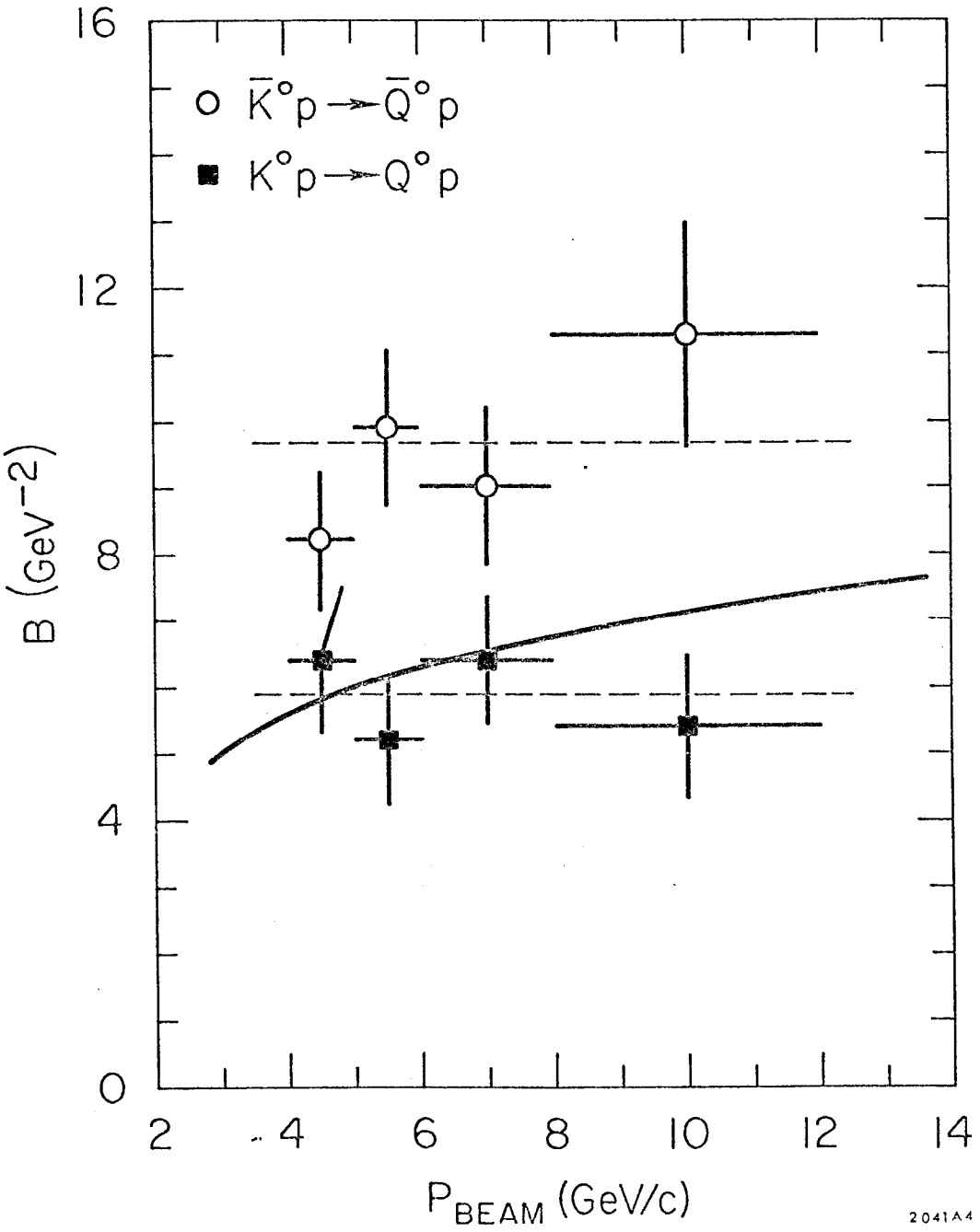
16
12
8
4
0
B (GeV^{-2})
○ $\bar{K}^0p \rightarrow \bar{Q}^0p$
■ $K^0p \rightarrow Q^0p$
2
4
6
8
10
12
14
P_{BEAM} (GeV/c)
2041A4

Fig. 9

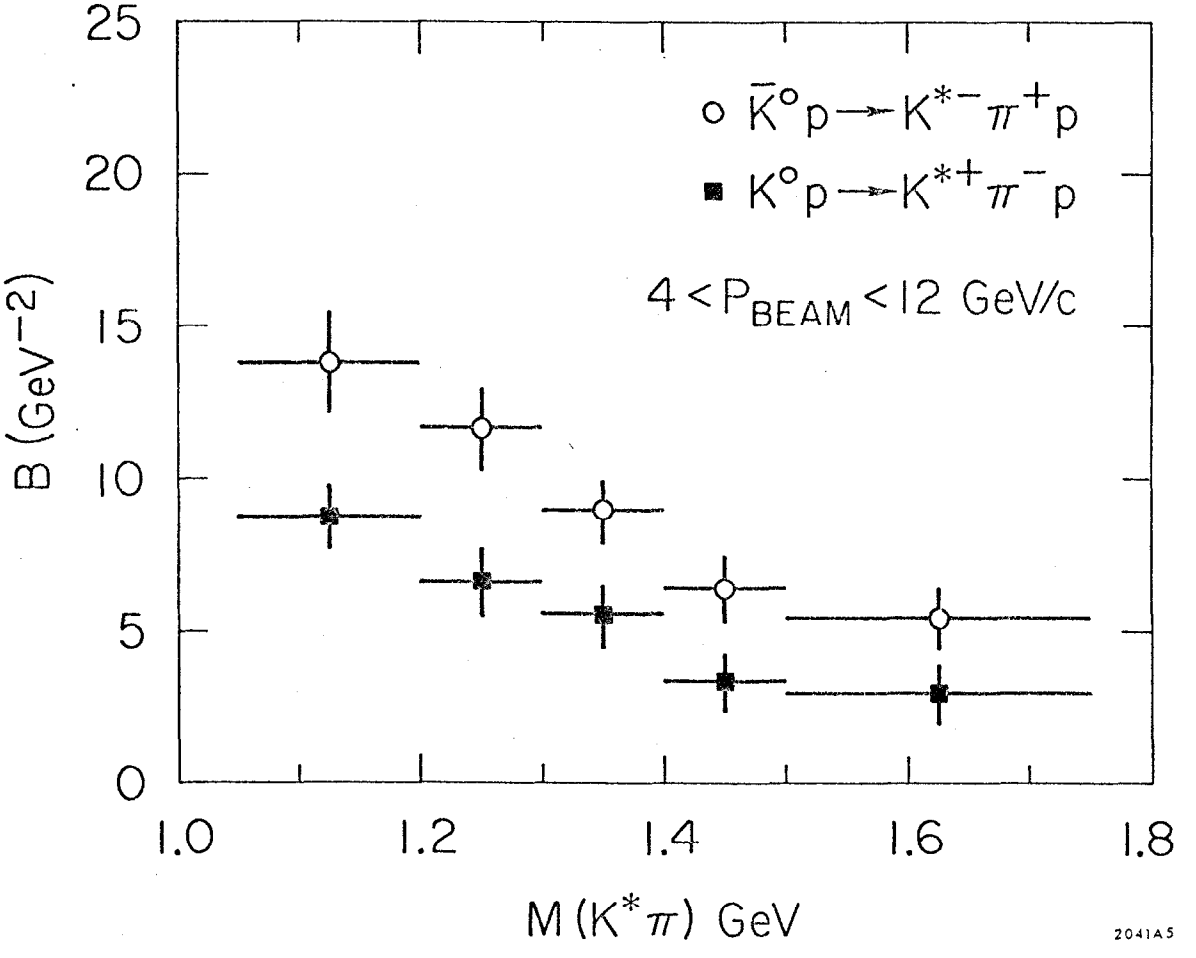
25
20
15
10
5
0
B (GeV^{-2})
1.0
1.2
1.4
1.6
1.8
M (K$^*\pi$) GeV
○ $\bar{K}^0 p \rightarrow K^{*-}\pi^+ p$
■ $K^0 p \rightarrow K^{*+}\pi^- p$
$4 < P_{BEAM} < 12$ GeV/c
2041A5

Fig. 10

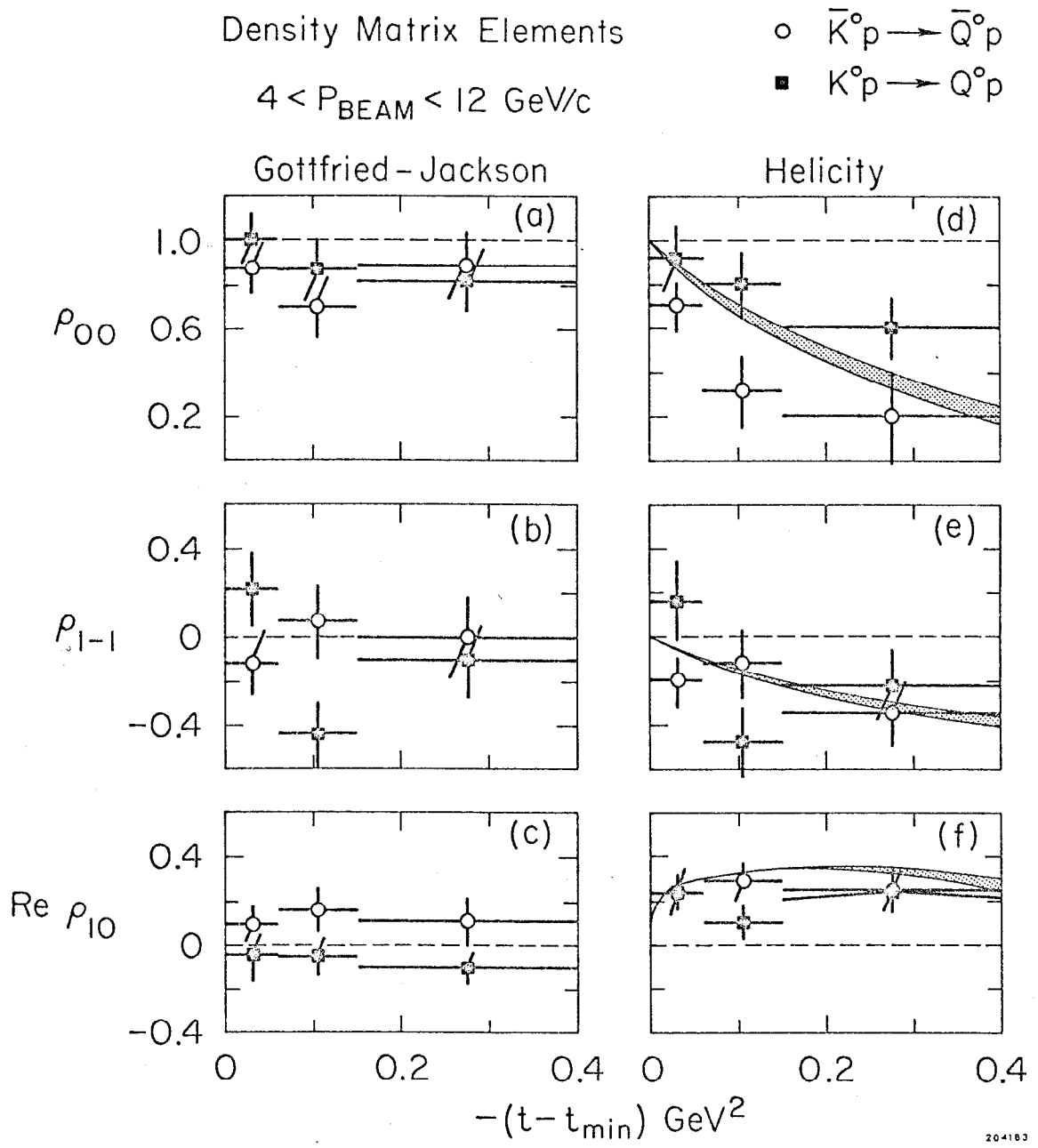
Density Matrix Elements
4 < P_BEAM < 12 GeV/c
o K̄°p → Q̄°p
■ K°p → Q°p
Gottfried-Jackson
Helicity
(a)
(b)
(c)
(d)
(e)
(f)
ρ00
ρ1-1
Re ρ10
1.0
0.6
0.2
0.4
0
-0.4
0
0.2
0.4
-(t-tmin) GeV2
204183

Fig. 11

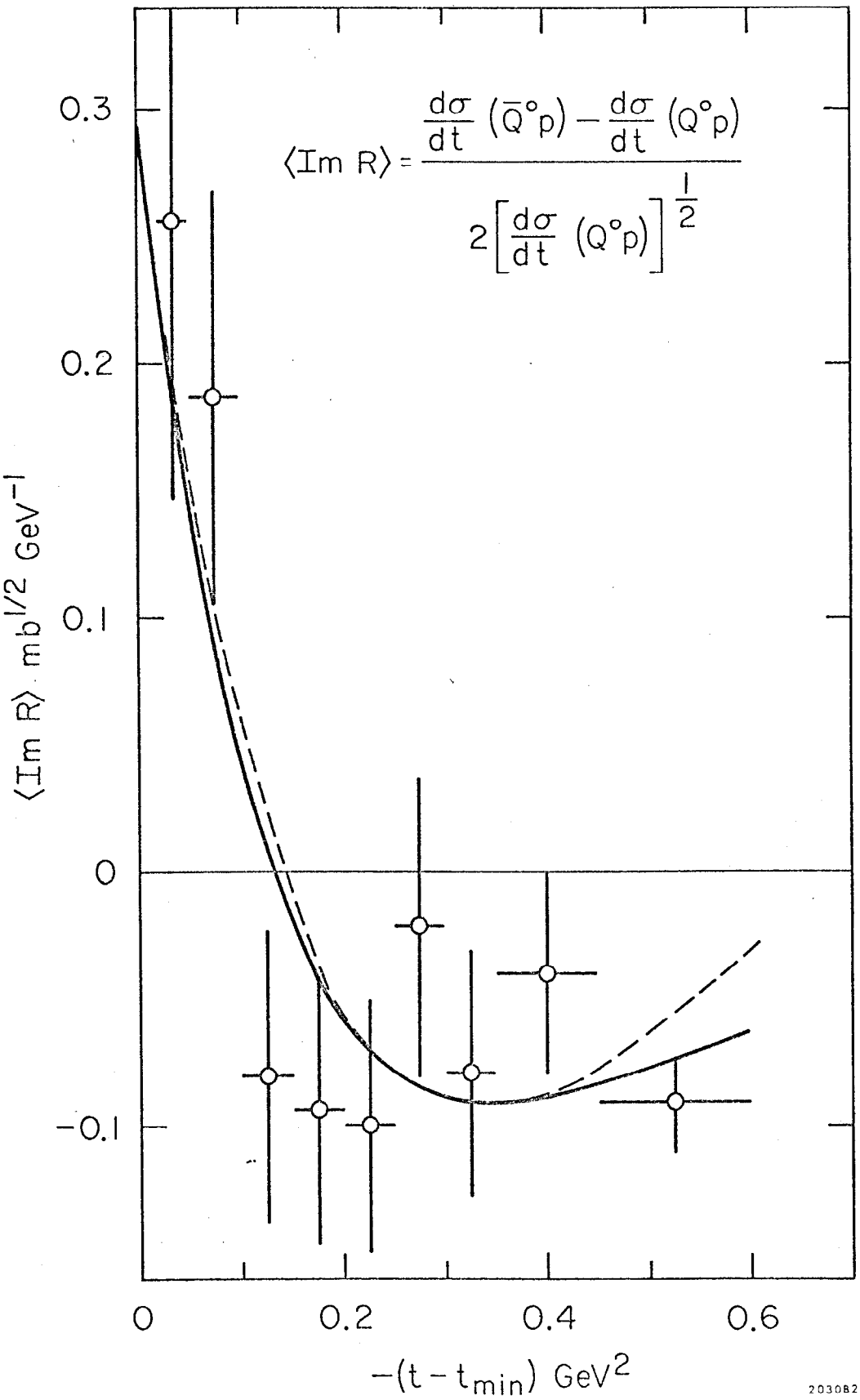
$\langle \text{Im } R \rangle = \dfrac{\frac{d\sigma}{dt}(\bar{Q}^\circ p) - \frac{d\sigma}{dt}(Q^\circ p)}{2\left[\frac{d\sigma}{dt}(Q^\circ p)\right]^{\frac{1}{2}}}$
0.3
0.2
0.1
0
-0.1
$\langle \text{Im } R \rangle$ mb$^{1/2}$ GeV^{-1}
0
0.2
0.4
0.6
$-(t - t_{min})$ GeV^2
203082

Fig. 12

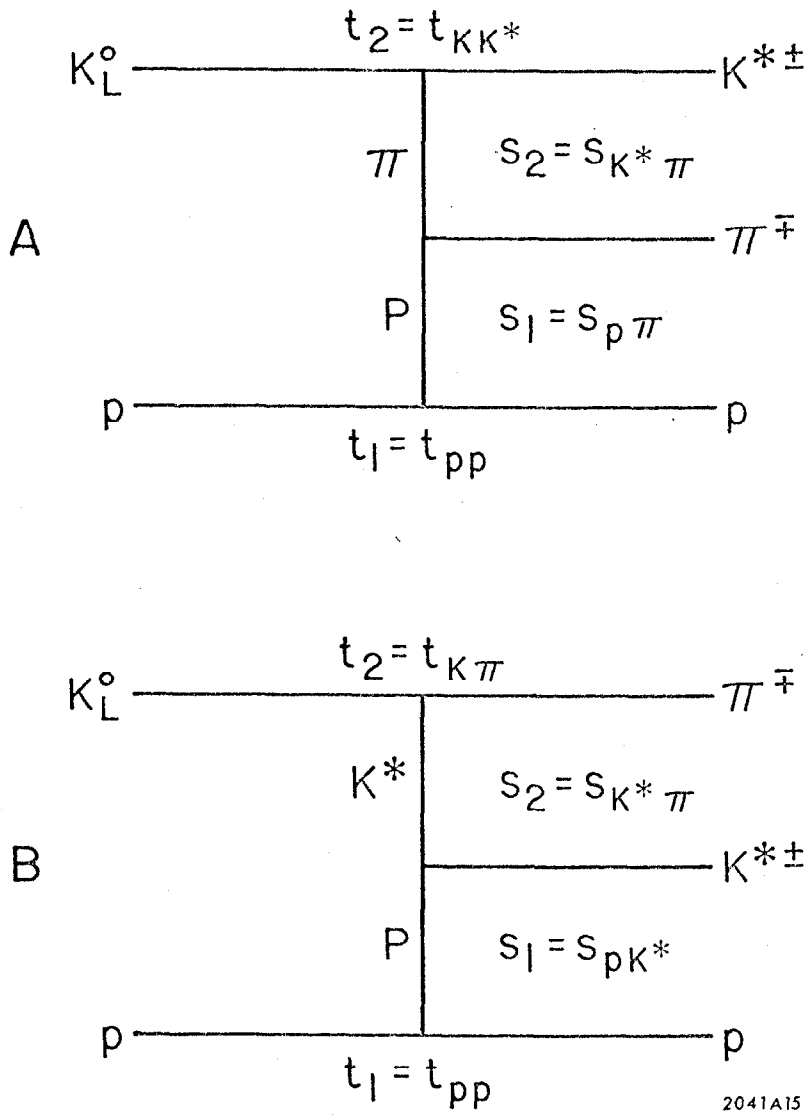
A
K^0_L
$t_2 = t_{K K^*}$
$K^{*\pm}$
π
$s_2 = s_{K^*\pi}$
$\pi^{\mp}$
P
$s_1 = s_{p\pi}$
p
p
$t_1 = t_{pp}$
B
K^0_L
$t_2 = t_{K\pi}$
$\pi^{\mp}$
K^*
$s_2 = s_{K^*\pi}$
$K^{*\pm}$
P
$s_1 = s_{pK^*}$
p
p
$t_1 = t_{pp}$
2041A15

Fig. 13

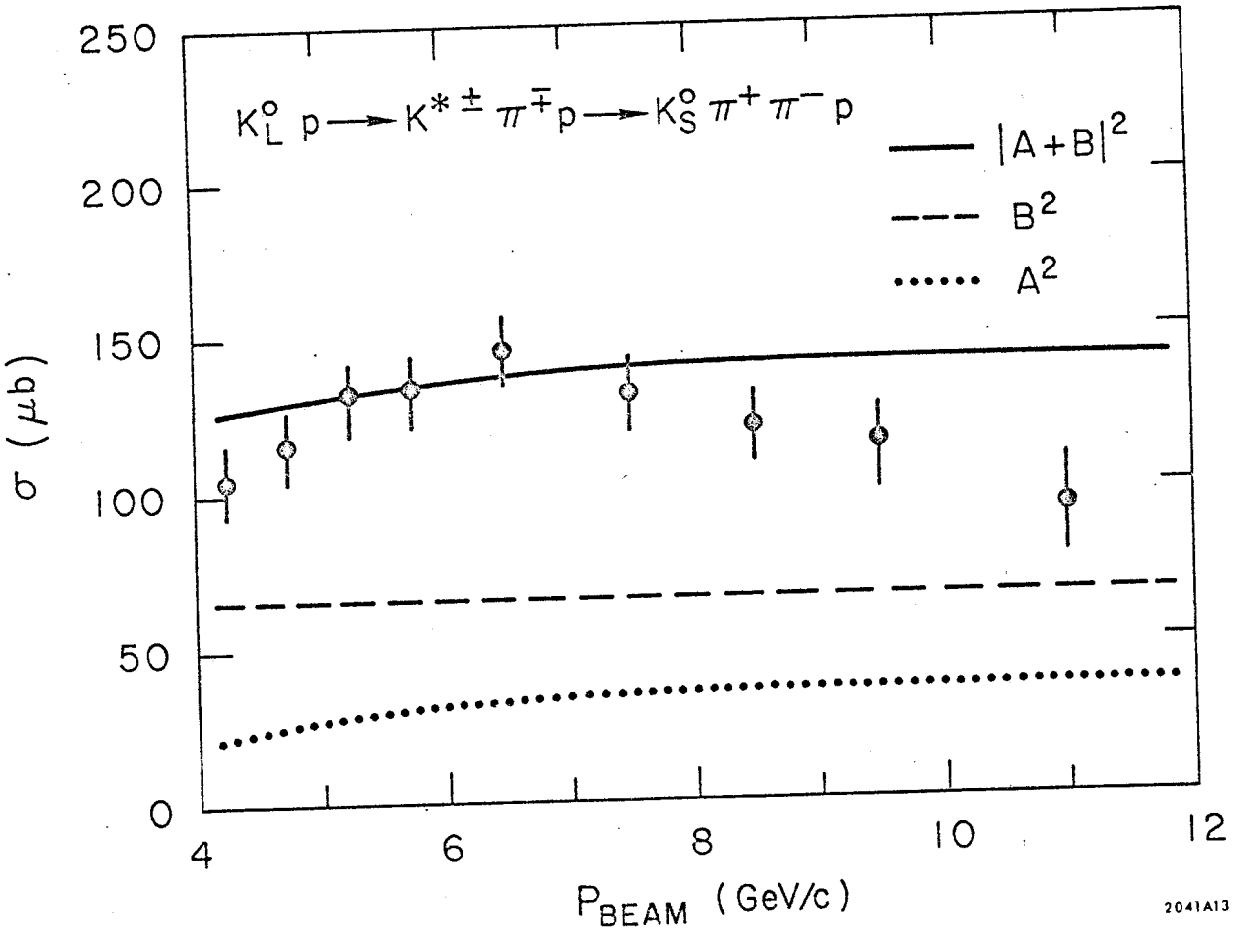
250
200
150
100
50
0
4
6
8
10
12
σ (μb)
$K^0_L\ p \rightarrow K^{*\pm}\pi^{\mp}p \rightarrow K^0_S\pi^+\pi^-p$
$|A+B|^2$
B^2
A^2
P_{BEAM} (GeV/c)
2041A13

Fig. 14

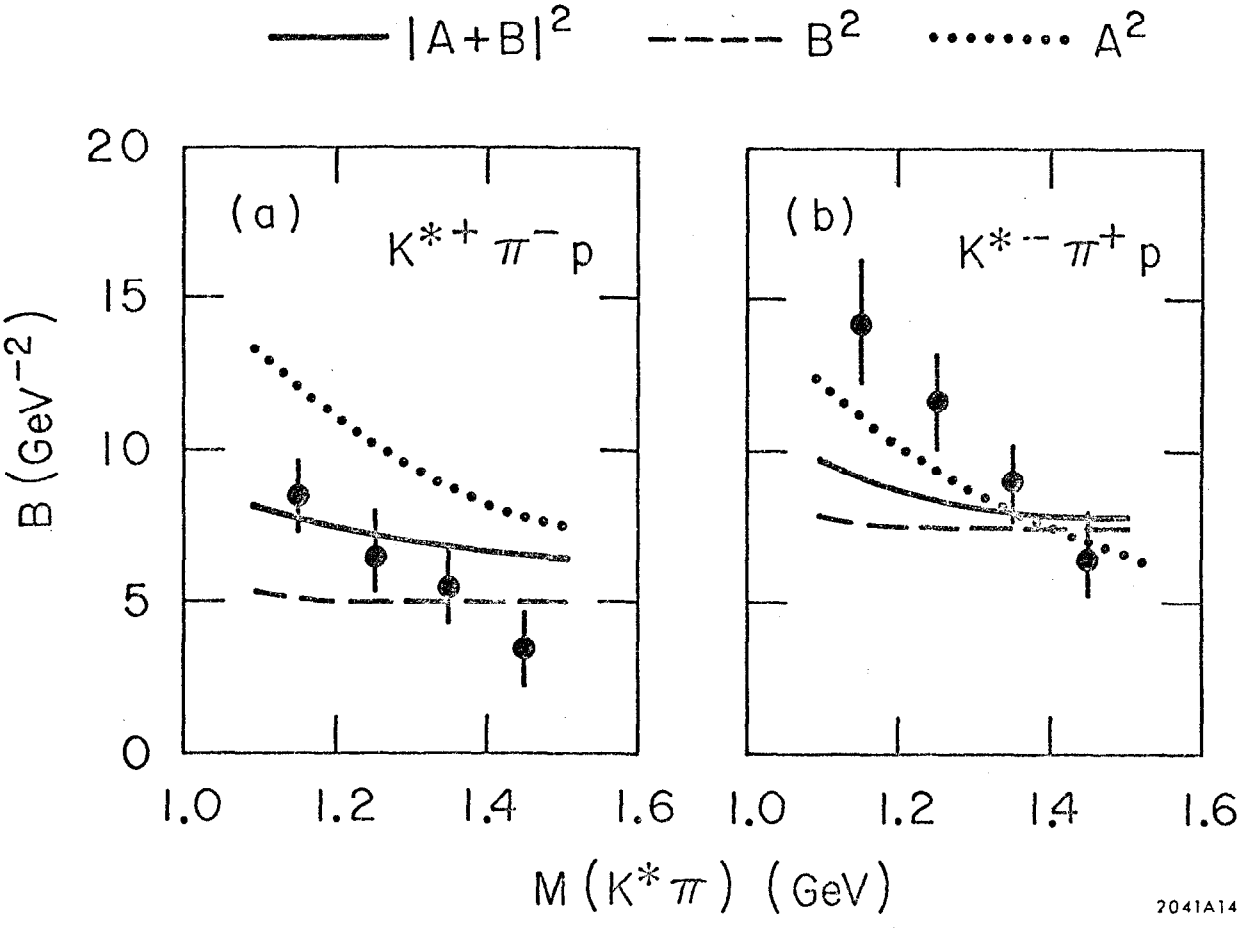
$|A+B|^2$
B^2
A^2
(a)
$K^{*+}\pi^-p$
(b)
$K^{*-}\pi^+p$
B (GeV^{-2})
20
15
10
5
0
1.0
1.2
1.4
1.6
M ($K^*\pi$) (GeV)
2041A14

Fig. 15